Inorg. Chem. **2006**, *45*, 17−36

Electronic Structure, Bonding, Spectroscopy and Energetics of Fe-Dependent Nitrile Hydratase Active-Site Models

Shannon N. Greene and Nigel G. J. Richards*

Department of Chemistry, University of Florida, Gainesville, Florida 32611-7200

Received June 14, 2005

Fe-type nitrile hydratase (NHase) is a non-heme Fe(III)-dependent enzyme that catalyzes the hydration of nitriles to the corresponding amides. Despite experimental studies of the enzyme and model Fe(III)-containing complexes, many questions concerning the electronic structure and spectroscopic transitions of the metal center remain unanswered. In addition, the catalytic mechanism of nitrile hydration has not yet been determined. We now report density functional theory (B3LYP/6-31G*) calculations on three models of the Fe(III) center in the active site of NHase corresponding to hypothetical intermediates in the enzyme-catalyzed hydration of acetonitrile. Together with natural bond orbital (NBO) analysis of the chemical bonding in these active-site models and INDO/S CIS calculations of their electronic spectra, this theoretical investigation gives new insight into the molecular origin of the unusual low-spin preference and spectroscopic properties of the Fe(III) center. In addition, the low-energy electronic transition observed for the active form of NHase is assigned to a dd transition that is coupled with charge-transfer transitions involving the metal and its sulfur ligands. Calculations of isodesmic ligand-exchange reaction energies provide support for coordination of the Fe(III) center in free NHase by a water molecule rather than a hydroxide ion and suggest that the activation of the nitrile substrate by binding to the metal in the sixth coordination site during catalytic turnover cannot yet be definitively ruled out.

Introduction

The biological hydration of nitriles to amides[1] is catalyzed by the enzyme nitrile hydratase (NHase), a non-heme/non-corrinoid metalloenzyme that contains either Fe(III) or Co(III) in the active site.[2] The initial biochemical interest in NHase was prompted by its utility for industrial acrylamide production and the enantioselective synthesis of primary amides.[3] The enzyme is generally more interesting to bioinorganic chemists, however, in that its active site contains either mononuclear, low-spin ($S = {}^1/_2$) Fe(III) or ($S = 0$) Co(III).[4] Because these ground-state spin preferences are not usually seen in metalloenzymes possessing non-heme Fe(III) or Co(III) centers,[5] this finding has stimulated the synthesis of numerous inorganic model complexes in efforts to understand the reactivity and spectroscopy of NHase.[5,6] Another intriguing chemical feature of Fe-type NHase is its

* Author to whom correspondence should be addressed. E-mail: richards@qtp.ufl.edu.

(1) (a) Lam, H. M.; Coschigano, K. T.; Oliveira, I. C.; Melo-Oliveira, R.; Coruzzi, G. M. *Annu. Rev. Plant Physiol. Plant Mol. Biol.* **1996**, *47*, 569−593. (b) Kobayashi, M.; Fujiwara, Y.; Goda, M.; Komeda, H.; Shimizu, S. *Proc. Natl. Acad. Sci. U.S.A.* **1997**, *94*, 11986−11991. (c) Stevenson, D. E.; Feng, R.; Dumas, F.; Groleau, D.; Mihoc, A.; Storer, A. C. *Biotechnol. Appl. Biochem.* **1992**, *15*, 283−302. (d) Stalker, D. M.; Malyj, L. D.; McBride, K. E. *J. Biol. Chem.* **1988**, *263*, 6310−6314. (e) Vennesland, B.; Castric, P. A.; Conn, E. E.; Solomonson, L. P.; Volini, M.; Westley, J. *Fed. Proc.* **1982**, *41*, 2639−2648. (f) Asano, Y.; Yasuda, T.; Tani, Y.; Yamada, H. *Agric. Biol. Chem.* **1982**, *46*, 1183−1189.

(2) (a) Endo, I.; Nojiri, M.; Tsujimura, M.; Nakasako, M.; Nagashima, S.; Yohda, M.; Odaka, M. *J. Inorg. Biochem.* **2001**, *83*, 247−253. (b) Kobayashi, M.; Shimizu, S. *Curr. Opin. Chem. Biol.* **2000**, *4*, 95−102. (c) Nakasako, M.; Odaka, M.; Yohda, M.; Dohmae, N.; Takio, K.; Kamiya, N.; Endo, I. *Biochemistry* **1999**, *38*, 9887−9898. (d) Nelson, M. J.; Jin, H.; Turner, I. M.; Grove, G.; Scarrow, R. C.; Brennan, B. A.; Que, L. *J. Am. Chem. Soc.* **1991**, *113*, 7072−7073. (e) Kopf, M.-A.; Bonnet, D.; Artaud, I.; Pétré, D.; Mansuy, D. *Eur. J. Biochem.* **1996**, *240*, 239−244. (f) Miyanaga, A.; Fushinobu, S.; Ito, K.; Shoun, H.; Wakagi, T. *Eur. J. Biochem.* **2004**, *271*, 429−438. (g) Payne, M. S.; Wu, S.; Fallon, R. D.; Tudor, G.; Stieglitz, B.; Turner, I. M.; Nelson, M. J. *Biochemistry* **1997**, *36*, 5447−5454. (h) Yamaki, T.; Oikawa, T.; Ito, K.; Nakamura, T. *J. Ferment. Bioeng.* **1997**, *83*, 474−477.

(3) (a) Endo, I.; Odaka, M.; Yohda, M. *Trends Biotechnol.* **1999**, *17*, 244−248. (b) Kobayashi, M.; Shimizu, S. *Nat. Biotechnol.* **1998**, *16*, 733−736. (c) Yamada, H.; Kobayashi, M. *Biosci. Biotechnol. Biochem.* **1996**, *60*, 1391−1400. (d) Kobayashi, M.; Nagasawa, T.; Yamada, H. *Trends Biotechnol.* **1992**, *10*, 402−408.

(4) (a) Sugiura, Y.; Kuwahara, J.; Nagasawa, T.; Yamada, H. *J. Am. Chem. Soc.* **1987**, *109*, 5848−5850. (b) Brennan, B. A.; Alms, G.; Nelson, M. J.; Durney, L. T.; Scarrow, R. C. *J. Am. Chem. Soc.* **1996**, *118*, 9194−9195. (c) Nojiri, M.; Nakayama, H.; Odaka, M.; Yohda, M.; Takio, K.; Endo, I. *FEBS Lett.* **2000**, *465*, 173−177.

(5) Kovacs, J. A. *Chem. Rev.* **2004**, *104*, 825−848.

10.1021/ic050965p CCC: $33.50
Published on Web 12/10/2005

ability to interact reversibly with nitric oxide (NO),[3a,7] a reaction that has been hypothesized to be important in the cellular regulation of the enzyme.[8] Thus, Fe-type NHase activity disappears in vivo due to the formation of a stable Fe−nitrosyl complex when cells containing the enzyme are kept in darkness. Reactivation of the enzyme is then accomplished by irradiation of NO-inactivated NHase with visible light, presumably due to photochemical cleavage of the Fe−NO bond.[3a,7,9]

High-resolution X-ray crystal structures have been reported for (i) the native, Fe-dependent NHase isolated from *Rhodococcus* sp. R312,[10a] (ii) an inactive, nitrosylated form of Fe-type NHase present in *Rhodococcus* sp. N-771,[10b] (iii) the cobalt-containing NHase from *Pseudonocardia thermophila* JCM 3095,[10c] and (iv) the Co-type nitrile hydratase present in *Bacillus smithii*.[10d] All four structures show that (i) NHase is composed of two subunits (α and β), (ii) the intact enzyme crystallizes as a dimer of heterodimers, and (iii) the active-site metal is octahedrally coordinated by three conserved cysteine residues, two deprotonated amide nitrogens from the protein backbone, and a sixth ligand. In agreement with mass spectrometric measurements,[11] two of these crystal structures[10b,10c] revealed a distinctive posttranslational modification of two thiolate ligands coordinating the metal in both the Fe- and Co-dependent forms of the enzyme, and oxidation of the side chain of Cys-112 in the α subunit to cysteine sulfinic (SO_2) acid was reported to be essential for catalytic activity in Fe-type NHase.[12] Recent computational studies by our group suggested a role for sulfur oxidation in facilitating Fe−NO bond cleavage[13] as a part of the molecular mechanisms that mediate photoregulation of NHase, although there is also experimental evidence that the enzyme is inhibited by "over-oxidation" of the sulfenate moiety that is derived from Cys-114 of the α subunit.[14] The functional role of sulfur oxidation in Fe-type NHase remains the subject of considerable uncertainty, however, despite the preparation and characterization of many model Fe(III) and Co(III) complexes.[6,15] In addition to these interesting structural features and the unique spin preference of the non-heme metal center, Fe-dependent NHase exhibits a characteristic, broad electronic absorption near 700 nm.[2d,16] It has been hypothesized that this low-energy band is associated with sulfur to iron charge transfer,[17] but no detailed study of the enzyme under well-defined conditions has yet been reported, and other absorption peaks in the electronic spectrum observed for active NHase remain unassigned.[9b,c]

The structure and unique electronic properties of the Fe(III) center in Fe-type NHase are remarkably complex in light of the relatively simple reaction that is catalyzed by the enzyme, raising questions about the roles of sulfur oxidation, metal coordination, and spin state in catalysis.[5,6] It is therefore surprising that systematic kinetic investigations have not been undertaken to elucidate the catalytic mechanism of NHase, especially in light of considerable speculation on this problem.[2,3,5,6,10] Moreover, experimental work employing inorganic Fe(III) complexes has yielded conflicting evidence

(6) (a) Harrop, T. C.; Mascharak, P. K. *Acc. Chem. Res.* **2004**, *37*, 253−260. (b) Mascharak, P. K. *Coord. Chem. Rev.* **2002**, *225*, 201−214. (c) Marlin, D. S.; Mascharak, P. K. *Chem. Soc. Rev.* **2000**, *29*, 69−74. (d) Artaud, I.; Chatel, S.; Chauvin, A. S.; Bonnet, D.; Kopf, M. A.; Leduc, P. *Coord. Chem. Rev.* **1999**, *190−192*, 577−586. (e) Sakurai, H.; Tsuchiya, K.; Migita, K. *Inorg. Chem.* **1988**, *27*, 3877−3879.

(7) (a) Odaka, M.; Fujii, K.; Hoshino, M.; Noguchi, T.; Tsujimura, M.; Nagashima, S.; Yohda, M.; Nagamune, T.; Inoue, Y.; Endo, I. *J. Am. Chem. Soc.* **1997**, *119*, 3785−3791. (b) Noguchi, T.; Hoshino, M.; Tsujimura, M.; Odaka, M.; Inoue, Y.; Endo, I. *Biochemistry* **1996**, *35*, 16777−16781.

(8) (a) Endo, I.; Odaka, M. *J. Mol. Catal. B: Enzym.* **2000**, *10*, 81−86. (b) Bonnet, D.; Artaud, I.; Moali, C.; Pétré, D.; Mansuy, D. *FEBS Lett.* **1997**, *409*, 216−220.

(9) (a) Noguchi, T.; Honda, J.; Nagamune, T.; Sasabe, H.; Inoue, Y.; Endo, I. *FEBS Lett.* **1995**, *358*, 9−12. (b) Honda, J.; Kandori, H.; Okada, T.; Nagamune, T.; Shichida, Y.; Sasabe, H.; Endo, I. *Biochemistry* **1994**, *33*, 3577−3583. (c) Honda, J.; Teratani, Y.; Kobayashi, Y.; Nagamune, T.; Sasabe, H.; Hirata, A.; Ambe, F.; Endo, I. *FEBS Lett.* **1992**, *301*, 177−180. (d) Popescu, V.-C.; Münck, E.; Fox, B. G.; Sanakis, Y.; Cummings, J. G.; Turner, I. M.; Nelson, M. J. *Biochemistry* **2001**, *40*, 7984−7991.

(10) (a) Huang, W.; Jia, J.; Cummings, J.; Nelson, M.; Schneider, G.; Lindqvist, Y. *Structure* **1997**, *5*, 691−699. (b) Nagashima, S.; Nakasako, M.; Dohmae, N.; Tsujimura, M.; Takio, K.; Odaka, M.; Yohda, M.; Kamiya, N.; Endo, I. *Nat. Struct. Biol.* **1998**, *5*, 347−351. (c) Miyanaga, A.; Fushinobu, S.; Ito, K.; Wakagi, T. *Biochem. Biophys. Res. Commun.* **2001**, *288*, 1169−1174. (d) Hourai, S.; Miki, M.; Takashima, Y.; Mitsuda, S.; Yanagi, K. *Biochem. Biophys. Res. Commun.* **2003**, *312*, 340−345.

(11) (a) Tsujimura, M.; Dohmae, N.; Odaka, M.; Chijimatsu, M.; Takio, K.; Yohda, M.; Hoshino, M.; Nagashima, S.; Endo, I. *J. Biol. Chem.* **1997**, *272*, 29454−29459. (b) Stevens, J. M.; Belghazi, M.; Jaouen, M.; Bonnet, D.; Schmitter, J.-M.; Mansuy, D.; Sari, M.-A.; Artaud, I. *J. Mass Spectrom.* **2003**, *38*, 955−961.

(12) (a) Lu, J.; Zheng, Y.; Yamagishi, H.; Odaka, M.; Tsujimura, M.; Maeda, M.; Endo, I. *FEBS Lett.* **2003**, *553*, 391−396. (b) Nojiri, M.; Yohda, M.; Odaka, M.; Matsushita, Y.; Tsujimura, M.; Yoshida, T.; Dohmae, N.; Takio, K.; Endo, I. *J. Biochem. (Tokyo)* **1999**, *125*, 696−704. (c) Murakami, T.; Nojiri, M.; Nakayama, H.; Odaka, M.; Yohda, M.; Dohmae, N.; Takio, K.; Nagamune, T.; Endo, I. *Protein Sci.* **2000**, *9*, 1024−1030.

(13) (a) Greene, S. N.; Richards, N. G. J. *Inorg. Chem.* **2004**, *43*, 7030−7041. (b) Greene, S. N.; Chang, C. H.; Richards, N. G. J. *Chem. Commun.* **2002**, 2386-2387.

(14) Tsujimura, M.; Odaka, M.; Nakayama, H.; Dohmae, N.; Koshino, H.; Asami, T.; Hoshino, M.; Takio, K.; Yoshida, S.; Maeda, M.; Endo, I. *J. Am. Chem. Soc.* **2003**, *125*, 11532−11538.

(15) (a) Grapperhaus, C. A.; Li, M.; Patra, A. K.; Poturovic, S.; Kozlowski, P. M.; Zgierski, M. Z.; Mashuta, M. S. *Inorg. Chem.* **2003**, *42*, 4382−4388. (b) Shearer, J.; Fitch, S. B.; Kaminsky, W.; Benedict, J.; Scarrow, R. C.; Kovacs, J. A. *Proc. Natl. Acad. Sci. U.S.A.* **2003**, *100*, 3671−3676. (c) Galardon, E.; Giorgi, M.; Artaud, I. *Chem. Commun.* **2004**, 286−287. (d) Lee, C.-M.; Hsieh, C.-H.; Dutta, A.; Lee, G.-H.; Liaw, W.-F. *J. Am. Chem. Soc.* **2003**, *125*, 11492−11493. (e) Patra, A. K.; Olmstead, M. M.; Mascharak, P. K. *Inorg. Chem.* **2002**, *41*, 5403−5409. (f) Moon, D.; Lah, M. S.; Del Sesto, R. E.; Miller, J. S. *Inorg. Chem.* **2002**, *41*, 4708−4714. (g) Grapperhaus, C. A.; Patra, A. K.; Mashuta, M. S. *Inorg. Chem.* **2002**, *41*, 1039−1041. (h) Chatel, S.; Chauvin, A.-S.; Tuchagues, J.-P.; Leduc, P.; Bill, E.; Chottard, J.-C.; Mansuy, D.; Artaud, I. *Inorg. Chim. Acta* **2002**, *336*, 19−28. (i) Jackson, H. L.; Shoner, S. C.; Rittenberg, D.; Cowen, J. A.; Lovell, S.; Barnhart, D.; Kovacs, J. A. *Inorg. Chem.* **2001**, *40*, 1646−1653. (j) Marlin, D. S.; Olmstead, M. M.; Mascharak, P. K. *Inorg. Chim. Acta* **2000**, *297*, 106−114. (k) Marlin, D. S.; Olmstead, M. M.; Mascharak, P. K. *Inorg. Chem.* **1999**, *38*, 3258−3260. (l) Noveron, J. C.; Herradora, R.; Olmstead, M. M.; Mascharak, P. K. *Inorg. Chim. Acta* **1999**, *285*, 269−276. (m) Noveron, J. C.; Olmstead, M. M.; Mascharak, P. K. *Inorg. Chem.* **1998**, *37*, 1138−1139. (n) Schweitzer, D.; Ellison, J. J.; Shoner, S. C.; Lovell, S.; Kovacs, J. A. *J. Am. Chem. Soc.* **1998**, *120*, 10996−10997. (o) Ellison, J. J.; Nienstedt, A.; Shoner, S. C.; Barnhart, D.; Cowen, J. A.; Kovacs, J. A. *J. Am. Chem. Soc.* **1998**, *120*, 5691−5700. (p) Nivorozhkin, A. L.; Uraev, A. I.; Bondarenko, G. I.; Antsyshkina, A. S.; Kurbatov, V. P.; Garnovskii, A. D.; Turta, C. I.; Brashoveanu, N. D. *Chem. Commun.* **1997**, 1711−1712.

(16) Nagasawa, T.; Ryuno, K.; Yamada, H. *Biochem. Biophys. Res. Commun.* **1986**, *139*, 1305−1312.

(17) Brennan, B. A.; Cummings, J. G.; Chase, D. B.; Turner, I. M., Jr.; Nelson, M. J. *Biochemistry* **1996**, *35*, 10068−10077.

concerning the likely intermediates in the NHase-catalyzed reaction.[5a,6] The problem is compounded for Fe-dependent NHase in that although several Co(III)-containing model complexes have been shown to catalyze the hydration of nitriles to amides,[18] Fe(III) complexes exhibiting similar reactivity have not been reported.[5a,19] In addition, efforts to obtain sulfinato derivatives (in which sulfur, rather than oxygen, is bound to the metal by oxidation of thiolates in Fe(III)-containing model complexes) have revealed an interesting dependence on the other ligands coordinating the metal,[15c,d,20] raising questions concerning the molecular mechanisms by which posttranslational oxidation of the NHase metal center is accomplished in vivo.[12]

With the availability of high-resolution (1.7 Å) structural information for the inactive, nitrosylated form of Fe-type NHase,[10b] density functional theory (DFT) calculations represent a complementary approach for investigating the electronic and spectroscopic properties of the active-site metal center.[21] Using methods that we have calibrated on a series of open-shell, Fe(III) model complexes,[22] we now report theoretical studies of the NHase active-site models **1**−**4** (Figure 1), which have been proposed as intermediates in the catalytic mechanism of the enzyme (Scheme 1). Our results provide new insight into how the unusual low-spin preference and spectroscopic properties of the Fe(III) center depend on the posttranslationally oxidized cysteine residues and deprotonated backbone amides that constitute the ligand field of the metal. Spectroscopic calculations also suggest that the origin of the unusual, low-energy, electronic transition observed for the active form of NHase can be assigned to a dd transition that is coupled with charge-transfer transitions involving the metal and its sulfur ligands. Moreover, calculations of isodesmic ligand-exchange reaction energies provide support for coordination of the Fe(III) center in free NHase by a water molecule rather than a hydroxide ion and suggest that the activation of the nitrile substrate by binding to the metal in the sixth coordination site during catalytic turnover cannot yet be definitively ruled out.

Computational Methods

Construction of Active-Site Models 1−4. The initial coordinates for each of the active-site model structures **1**−**4** (Figure 1) were based on the X-ray crystal structure of the inactive, nitrosylated form of NHase present in *Rhodococcus* sp. N-771 (Protein Data Bank entry code: 1J58).[10b] Thus, atoms defining the active site were excised following a procedure identical to that reported in our previous studies of the role of posttranslational modification in NHase.[13] The inclusion of the side chains of two conserved arginines (Arg-56, Arg-141) in the β subunit, which form hydrogen bonds to the oxidized sulfur ligands of the Fe(III) center, is an important feature of the active-site models employed in these studies. Both guanidinium moieties, together with the ends of the α-subunit peptide chain containing the metal ligands, were capped with methyl groups (Figure 1), and the distances between the four carbon atoms in these methyl groups were fixed at their crystallographic values so as to prevent significant distortions of the active-site model structures during geometry optimization. The initial coordinates for active-site model **1** were then obtained by deletion of the NO ligand. In the case of **2**, the initial coordinates were obtained from an optimized active-site model of nitrosylated NHase (described previously in our studies of posttranslational oxidation in the photoregulation of enzyme activity[13b]) by the replacement of NO with a water molecule. After constrained geometry optimization of this water model at its low-spin state (see below), the initial coordinates for active-site models **3** and **4** were generated by the replacement of water with either hydroxide (**3**) or acetonitrile (**4**).

Geometry Optimization of Active-Site Models. Spin-unrestricted geometry optimizations of the active-site model structures **1**−**4** were performed using the BLYP exchange-correlation functional[23,24] with a 6-31G* basis set,[25] as implemented in the TURBOMOLE package.[26] The converged BLYP MO coefficients were employed as initial guesses for subsequent single-point energy calculations on the models at their BLYP-optimized geometries with unrestricted B3LYP[27,28] with the third form of the VWN local correlation functional (VWN-III),[29] as implemented in *Gaussi-*

(18) (a) Tyler, L. A.; Noveron, J. C.; Olmstead, M. M.; Mascharak, P. K. *Inorg. Chem.* **2003**, *42*, 5751−5761. (b) Heinrich, L.; Mary-Verla, A.; Li, Y.; Vaissermann, J.; Chottard, J.-C. *Eur. J. Inorg. Chem.* **2001**, 2203−2206. (c) Noveron, J. C.; Olmstead, M. M.; Mascharak, P. K. *J. Am. Chem. Soc.* **1999**, *121*, 3553−3554.

(19) In this regard, we note that one Fe(III) complex, prepared as a model of the active-site metal center in NHase, has been shown to bind nitriles reversibly. See: Shearer, J.; Jackson, H. L.; Schweitzer, D.; Rittenberg, D. K.; Leavy, T. M.; Kaminsky, W.; Scarrow, R. C.; Kovacs, J. A. *J. Am. Chem. Soc.* **2002**, *124*, 11417−11428.

(20) (a) Noveron, J. C.; Olmstead, M. M.; Mascharak, P. K. *J. Am. Chem. Soc.* **2001**, *123*, 3247−3259. (b) Tyler, L. A.; Noveron, J. C.; Olmstead, M. M.; Mascharak, P. K. *Inorg. Chem.* **1999**, *38*, 616−617. (c) Heinrich, L.; Li, Y.; Vaissermann, J.; Chottard, G.; Chottard, J.-C. *Angew. Chem., Int. Ed.* **1999**, *38*, 3526−3528. (l)

(21) (a) Solomon, E. I.; Szilagyi, R. K.; DeBeer George, S.; Basumallick, L. *Chem. Rev.* **2004**, *104*, 419−458. (b) Bassan, A.; Blomberg, M. R. A.; Borowski, T.; Siegbahn, P. E. M. *J. Phys. Chem. B* **2004**, *108*, 13031−13041. (c) Friesner, R. A.; Baik, M.-H.; Gherman, B. F.; Guallar, V.; Wirstam, M.; Murphy, R. B.; Lippard, S. J. *Coord. Chem. Rev.* **2003**, *238*−*239*, 267−290. (d) Ghosh, A.; Steene, E. *J. Biol. Inorg. Chem.* **2001**, *6*, 739−752. (e) Harris, D. L. *Curr. Opin. Chem. Biol.* **2001**, *5*, 724−735. (f) Spiro, T. G.; Zgierski, M. Z.; Kozlowski, P. M. *Coord. Chem. Rev.* **2001**, *219*−*221*, 923−936. (g) Li, S.; Hall, M. B. *Inorg. Chem.* **2001**, *40*, 18−24. (h) Siegbahn, P. E. M.; Blomberg, M. R. A. *Chem. Rev.* **2000**, *100*, 421−437. (i) Siegbahn, P. E. M. *Adv. Chem. Phys.* **1996**, *93*, 333−387. (j) Siegbahn, P. E. M.; Blomberg, M. R. A. *Annu. Rev. Phys. Chem.* **1999**, *50*, 221−249.

(22) (a) Chang, C. H.; Boone, A. J.; Bartlett, R. J.; Richards, N. G. J. *Inorg. Chem.* **2004**, *43*, 458−472. (b) Boone, A. J.; Chang, C. H.; Greene, S. N.; Herz, T.; Richards, N. G. J. *Coord. Chem. Rev.* **2003**, *238*−*239*, 291−314. (c) For recent ONIOM (DFT:PM3) calculations on these Fe(III) model complexes, see: Morgado, C. A.; McNamara, J. P.; Hillier, I. H.; Sundararajan, M. *Mol. Phys.* **2005**, *103*, 905−923. (d) For additional information on the performance of DFT functionals in modeling the spin-state-dependent properties of Fe(III)-containing systems, see: Swart, M.; Groenhof, A. R.; Ehlers, A. W.; Lammertsma, K. *J. Phys. Chem. A* **2004**, *108*, 5479−5483; Swart, M.; Ehlers, A. W.; Lammertsma, K. *Mol. Phys.* **2004**, *102*, 2467−2474; Deeth, R. J.; Fey, N. *J. Comput. Chem.* **2004**, *25*, 1840−1848.

(23) Becke, A. D. *Phys. Rev. A: At., Mol., Opt. Phys.* **1988**, *38*, 3098−3100.

(24) Lee, C.; Yang, W.; Parr, R. G. *Phys. Rev. B*: *Condens. Matter Mater. Phys.* **1988**, *37*, 785−789.

(25) (a) Hehre, W. J.; Ditchfield, R.; Pople, J. A. *J. Chem. Phys.* **1972**, *56*, 2257−2261. (b) Hariharan, P. C.; Pople, J. A. *Theor. Chim. Acta* **1973**, *28*, 213−222. (c) Francl, M. M.; Pietro, W. J.; Hehre, W. J.; Binkley, J. S.; Gordon, M. S.; DeFrees, D. J.; Pople, J. A. *J. Chem. Phys.* **1982**, *77*, 3654−3665. (d) Rassolov, V. A.; Pople, J. A.; Ratner, M. A.; Windus, T. L. *J. Chem. Phys.* **1998**, *109*, 1223−1229. (e) Feller, D.; Davidson, E. R. In *Reviews in Computational Chemistry*; Lipkowitz, K. B., Boyd, D. B., Eds.; VCH: New York, 1990; Vol. 1, pp 1−43.

(26) (a) Von Arnim, M.; Ahlrichs, R. *J. Comput. Chem.* **1998**, *19*, 1746−1757. (b) Ahlrichs, R.; Bär, M.; Häser, M.; Horn, H.; Kölmel, C. *Chem. Phys. Lett.* **1989**, *162*, 165−169.

(27) Becke, A. D. *J. Chem. Phys.* **1993**, *98*, 5648−5652.

(28) Stephens, P. J.; Devlin, F. J.; Chabalowski, C. F.; Frisch, M. J. *J. Phys. Chem.* **1994**, *98*, 11623−11627.

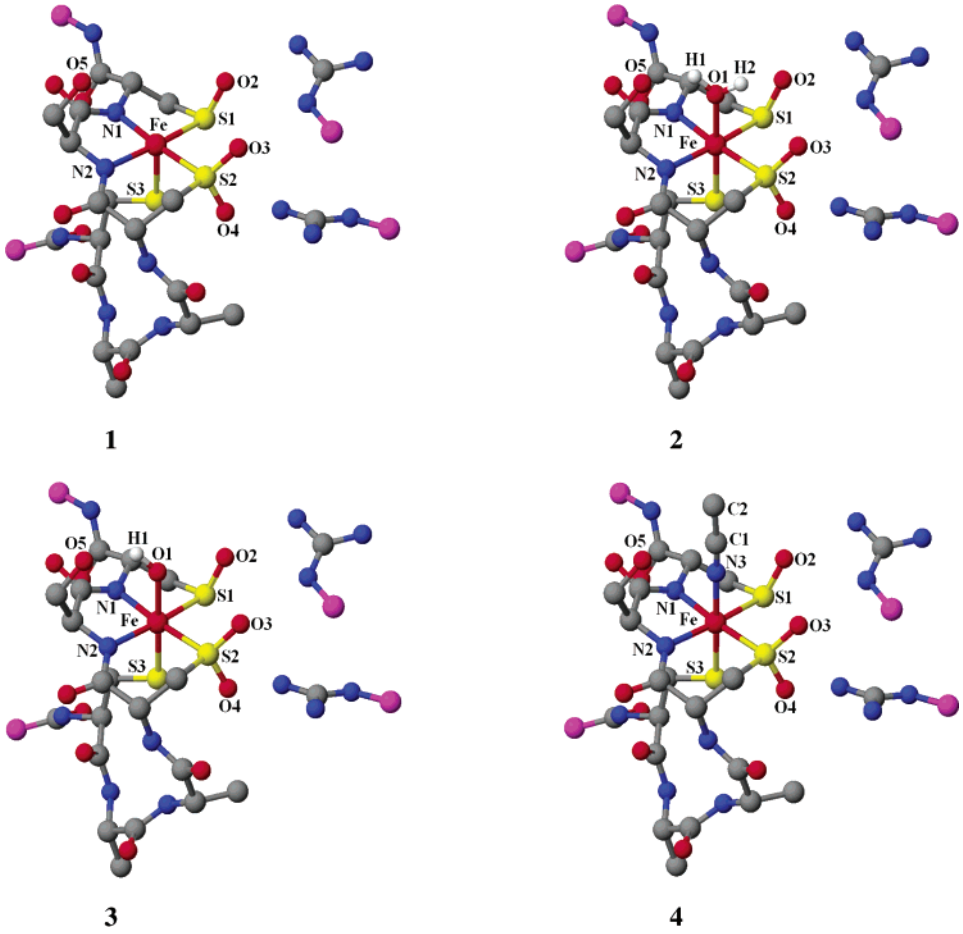

Figure 1. NHase active-site model structures **1**−**4** used in this study. The positions of the carbon atoms highlighted in purple were "frozen" with respect to the Fe(III) center and each other during geometry optimization. For clarity, non-hydrogen atoms are principally shown, and atoms are colored using the following scheme: C, black; H, white; N, blue; O, red; S, yellow; Fe, red. These structures were visualized using the CAChe Worksystem Pro V6.0 software package.

Scheme 1. Initial Steps of One Hypothetical Mechanism for Fe-Type NHase-Catalyzed Nitrile Hydration,[10] Showing Schematic Representations of the Active-Site Models **1**−**4** Investigated in This Hybrid DFT Study

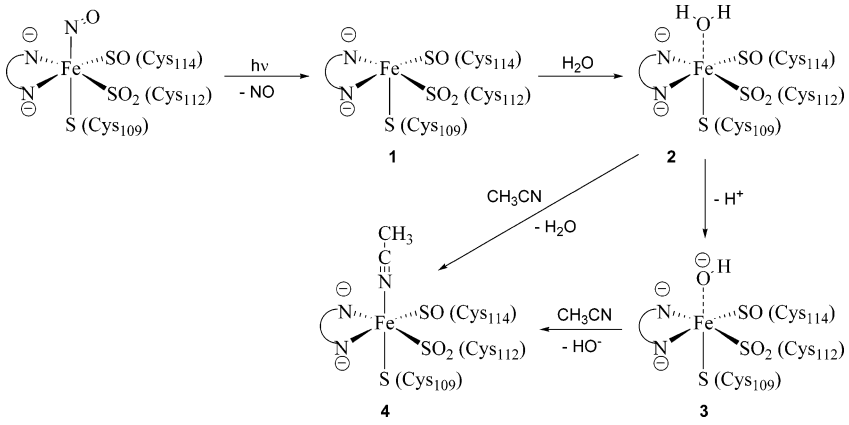

an98.[30] The latter calculations also employed a 6-31G* basis, which gives excellent geometries and electronic structures for related, non-heme Fe(III) complexes with N/S coordination, as we have shown.[22] The density matrix in all single-point energy calculations was converged to a tight RMS threshold of 10^{-8} au, and geometry optimizations were converged to a gradient of 10^{-3} hartree/bohr. Stability checks were performed on the DFT wave functions computed for all four NHase active-site models.

The extent of spin contamination in the DFT wave functions for these open-shell, Fe(III)-containing active-site models was estimated on the basis of the noninteracting values of $\langle S^2\rangle_{KS}$, as evaluated in TURBOMOLE and *Gaussian98* for the unrestricted BLYP/6-31G* and B3LYP/6-31G* calculations, respectively. We have discussed the validity and limitations of employing the value of $\langle S^2\rangle_{KS}$ as

(29) Vosko, S. H.; Wilk, L.; Nusair, M. *Can. J. Phys.* **1980**, *58*, 1200−1211.
(30) Frisch, M. J.; et al. *Gaussian 98*, Revision A.7; Gussian: Pittsburgh, PA, 1998.

computed from a single determinant of Kohn−Sham orbitals elsewhere.[22b] In an effort to identify the spatial location of any spin polarization, we computed spin magnetization densities (SMD) (ρ^{SMD}) using the following equation:

$$\rho^{SMD} = \rho^{\alpha} - \rho^{\beta}$$

[31] These calculations, together with graphical visualization of the SMD, were performed using CAChe Worksystem Pro V6.1 (CAChe Group, Biosciences Division, Fujitsu, Beaverton, OR).

NBO Analysis of Kohn−Sham Wave Functions for the NHase Active-Site Models. Kohn−Sham wave functions determined for the BLYP-optimized structures were analyzed within the natural bond orbital formalism[32] using the NBO 5.0 package.[33] Input files for this analysis were obtained by performing single-point energy calculations on each of the active-site models at its BLYP-optimized geometry using a B3LYP/LACVP* model chemistry, as implemented in Jaguar V5.0 (Schrödinger LLC, Portland, OR). Thus, an effective core potential[34] was used on Fe together with a 6-31G* basis on all other atoms. The initial guess of the density in these calculations was obtained from an algorithm based upon the ligand-field theory and dd repulsion,[35] and the density matrix and energy for all B3LYP/LACVP* calculations were converged to an RMS of 10^{-7} au and 10^{-6} hartrees, respectively. The extent of covalency in metal−ligand bonds was evaluated by analysis of the natural localized molecular orbitals (NLMOs)[36] and natural bond orbitals (NBOs) using a similar procedure to that reported previously for open-shell Fe(III) complexes.[22a] Atomic charges and populations were derived from natural population analysis (NPA).[37]

Spectroscopic Calculations on NHase Active-Site Models 2−4. Electronic transition energies and oscillator strengths were calculated for the lowest-energy spin state of active-site models **2**−**4** at their BLYP-optimized, gas-phase geometries using the semiempirical INDO/S CI singles (CIS) approximation.[38,39] All INDO/S calculations employed a β_d value of −23.0 eV for iron[38a] and standard resonance integrals and interaction factors ($f_{p\sigma p\sigma} = 1.267$ and $f_{p\pi p\pi} = 0.585$).[38b,38c] The CIS calculation for each model structure included all singly excited configurations from a restricted open-shell Hartree−Fock (ROHF) ground-state reference determinant, with active spaces being chosen on the basis of an initial CI employing all occupied, heavy-atom valence MOs on atoms in residues bonded directly to the metal and the two active-site arginines being excited into all virtual MOs of lower energy than that composed principally of Fe 4p orbitals. Configurations within 50 000 cm^{-1} of the ground state identified in this preliminary computation were then used to define the CI active space in subsequent spectroscopic calculations. Gaussian broadening of the calculated absorption energies and oscillator strengths, using a bandwidth of 3200 cm^{-1}, was performed to facilitate comparison of theoretical and experimental spectra. Similar procedures have been used in previous theoretical studies of other iron-containing complexes.[13,40]

Scheme 2[a]

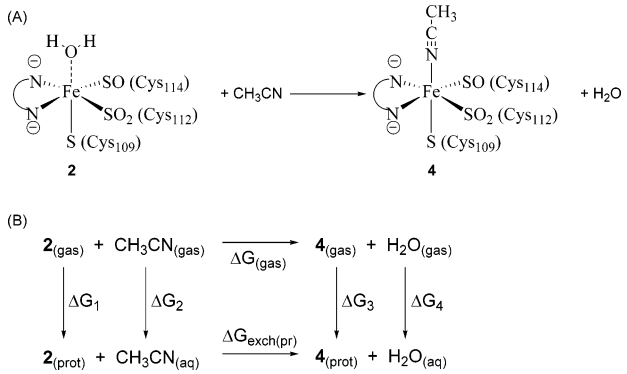

[a] (A) Isodesmic reaction for replacement of water by acetonitrile in the NHase active-site models. (B) Thermodynamic cycle employed in these calculations to obtain the energy for binding acetonitrile in place of water in the NHase active site. Subscripts (prot) and (aq) refer to the protein environment and aqueous solution, respectively.

Ligand-Exchange Calculation. The ligand-exchange energy ($\Delta G_{exch(pr)}$) was computed for an isodesmic reaction[41] involving active-site models **2** and **4** (Scheme 2). Gas-phase energies for acetonitrile, water, and the active-site models **2** and **4** were obtained using the B3LYP functional and a LACV3P++ basis set, as implemented in Jaguar V5.0, for the models at their lowest-energy BLYP/6-31G*-optimized geometry. Zero-point energy and thermal corrections to the Gibbs free energy were then computed for the gas-phase NHase models **2** and **4**, using truncated active sites that included iron, the amide nitrogens, the sulfinate and protonated sulfenate moieties, the axial thiolate sulfur, and the appropriate ligand in the sixth coordination site (Figure S1, Supporting Information), with the remaining atoms of each model being included in the calculation as counterpoise atoms. The effect of the protein environment on the energies of the two active-site models (ΔG_1 and ΔG_3) was estimated using a self-consistent reaction field (SCRF) model[42,43] for which the values of the dielectric constant (ϵ) and probe radius were 20 and 1.4 Å, respectively (Scheme 2B). This choice reflects the fact that the Fe(III) center in both crystal structures of NHase is easily accessible to water, making it likely that the active site is well solvated in the free enzyme.[2c] The energy of transferring acetonitrile (ΔG_2) or water

(31) Ziegler, T. *Can. J. Chem.* **1995**, *73*, 743−761.
(32) (a) Weinhold, F. In *Encyclopedia of Computational Chemistry*; Schleyer, P. v. R., Allinger, N. L., Clark, T., Gasteiger, J., Kollman, P. A., Schaefer, H. F., III, Schreiner, P. R., Eds.; Wiley: Chichester, 1998; pp 1792−1811. (b) Reed, A. E.; Curtiss, L. A.; Weinhold, F. *Chem. Rev.* **1988**, *88*, 899−926.
(33) Glendening, E. D.; Badenhoop, J. K.; Reed, A. E.; Carpenter, J. E.; Bohmann, J. A.; Morales, C. M.; Weinhold, F. *NBO 5.0*; Theoretical Chemistry Institute, University of Wisconsin: Madison, WI, 2001.
(34) Hay, P. J.; Wadt, W. R. *J. Chem. Phys.* **1985**, *82*, 299−310.
(35) Vacek, G.; Perry, J. K.; Langlois, J.-M. *Chem. Phys. Lett.* **1999**, *310*, 189−194.
(36) Reed, A. E.; Weinhold, F. *J. Chem. Phys.* **1985**, *83*, 1736−1740.
(37) Reed, A. E.; Weinstock, R. B.; Weinhold, F. *J. Chem. Phys.* **1985**, *83*, 735−746.
(38) (a) Zerner, M. C.; Loew, G. H.; Kirchner, R. F.; Mueller-Westerhoff, U. T. *J. Am. Chem. Soc.* **1980**, *102*, 589−599. (b) Bacon, A. D.; Zerner, M. C. *Theor. Chim. Acta* **1979**, *53*, 21−54. (c) Ridley, J.; Zerner, M. *Theor. Chim. Acta* **1973**, *32*, 111−134. (d) Zerner, M. C. In *Reviews in Computational Chemistry*; Lipkowitz, K. B., Boyd, D. B., Eds.; VCH: New York, 1991; Vol. 2, pp 313−365.
(39) All INDO/S calculations were performed using in-house software packages at the Quantum Theory Project, University of Florida.
(40) (a) Kotzian, M.; Rösch, N.; Schröder, H.; Zerner, M. C. *J. Am. Chem. Soc.* **1989**, *111*, 7687−7696. (b) Loew, G. H.; Harris, D. L. *Chem. Rev.* **2000**, *100*, 407−419. (c) Cory, M. G.; Stavrev, K. K.; Zerner, M. C. *Int. J. Quantum Chem.* **1997**, *63*, 781−795.
(41) Cramer, C. J. *Essentials of Computational Chemistry*; Wiley: New York, 2002.
(42) Tannor, D. J.; Marten, B.; Murphy, R.; Friesner, R. A.; Sitkoff, D.; Nicholls, A.; Ringnalda, M.; Goddard, W. A., III; Honig, B. *J. Am. Chem. Soc.* **1994**, *116*, 11875−11882.
(43) For overviews of the theoretical basis of SCRF models and their use in computational chemistry, see: (a) Orozco, M.; Luque, F. J. *Chem. Rev.* **2000**, *100*, 4187−4225. (b) Cramer, C. J.; Truhlar, D. G. *Chem. Rev.* **1999**, *99*, 2161−2200. (c) Bashford, D.; Case, D. A. *Annu. Rev. Phys. Chem.* **2000**, *51*, 129−152. (d) Tomasi, J.; Persico, M. *Chem. Rev.* **1994**, *94*, 2027−2094.

Scheme 3[a]

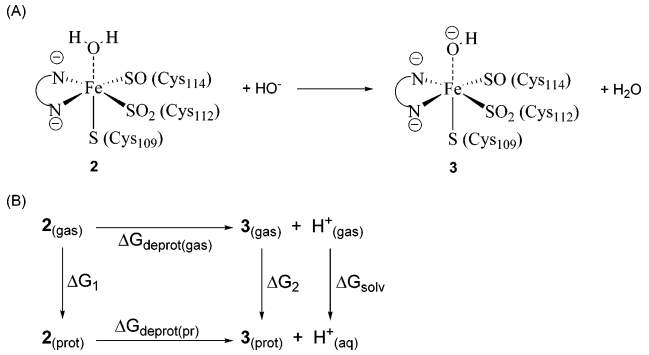

[a] (A) Conversion of NHase active-site model **2** to yield **3** by deprotonation of metal-bound water. (B) Thermodynamic cycle employed to compute the pK_a of the metal-bound water in active-site model **2**. Subscripts (prot) and (aq) refer to the protein environment and aqueous solution, respectively.

(ΔG_4) from the gas phase to aqueous solution was computed using the same SCRF model, except that a dielectric constant of 80.37 was used in the calculation.[44] The gas-phase calculations employed a standard state of 1 atm and 298.15 K, whereas determinations of the solvation free energies used a standard state of 1 M and, hence, include an additional 1.89 kcal/mol (see Supporting Information).[41]

Estimation of the pK_a of the Metal-Bound Water in Active-Site Model 2. The free energy required for deprotonation of the Fe-bound water in **2** to yield NHase active-site model **3** (Scheme 3A) was computed using standard literature methods (Scheme 3B).[45] Experimental values of −262.23 and −6.28 kcal/mol were chosen for the energy released on transferring a proton from the gas phase to aqueous solution (ΔG_{solv})[46] and the free energy of a proton in the gas phase,[47] respectively. As in the calculation of ligand-exchange energies, the effect of the protein environment on the energy of active-site model **3** (ΔG_2) was estimated using the SCRF model[43] implemented in Jaguar V5.0 with $\epsilon = 20$. The desired pK_a value was then obtained from the calculated free energy change ($\Delta G_{deprot(pr)}$) using the following equation:

$$\mathrm{p}K_a = \frac{1}{2.303RT}\Delta G^0_{\mathrm{deprot(pr)}}$$

where T is 298.15 K and R is the ideal gas constant. Energetic corrections were included to account for the choice of standard states, which were identical to those used in the calculations of ligand-exchange free energy discussed above.

Results and Discussion

Vertical Transition Energies of NHase Active-Site Models 1−4. Spin-unrestricted geometry optimizations of the active-site model structures **1**−**4** in their doublet spin states ($S = {}^1/_2$) were performed using the BLYP exchange-correlation functional[23,24] with a 6-31G* basis set.[25] Vertical transition energies were then computed for all four models using the same atomic orbital (AO) basis and the B3LYP functional implemented in *Gaussian98* (Table S1, Supporting Information). Our main goals in performing these calculations were (i) to obtain a rough estimate of the d-orbital splitting on the Fe(III) center and, hence, a qualitative measure of the ligand-field (LF) strengths of the residues defining the first coordination sphere and (ii) to evaluate the extent to which the DFT wave functions for these models might exhibit spin contamination. On this point, we have shown that the B3LYP functional correctly predicts the ground-state spin preferences for a series of Fe(III) complexes with ligands similar to those coordinating the metal in the NHase active site.[22a] On the basis of B3LYP single-point energy calculations, the LF splitting was smallest in the five-coordinate active-site model **1**, as might be expected on the basis of crystal field theory. The vertical transition energies computed for **2** and **3** are also consistent with known LF strengths, wherein water is a stronger field ligand than hydroxide.[48] The low-spin ($M_S = {}^1/_2$) state was of lowest energy for all four NHase active-site models, and the amount of spin contamination (at least as measured by the value of $\langle S^2\rangle_{KS}$ computed from a single determinant of Kohn−Sham orbitals)[22b] was minimal even at spin states for which the molecular geometry was nonoptimal (Table S1). To determine the spatial localization (if any) of the excess spin, we examined the spin magnetization density (SMD) of all calculated M_S states for each model at its doublet geometry (Figure 2). In **2**−**4**, for which the values of $\langle S^2\rangle_{KS}$ suggested little spin contamination, the unpaired (α) spin was localized primarily within the Fe d_{yz} orbital. A small amount of spin density was observed on the hydroxide oxygen and the carboxamido nitrogen atoms in active-site models **3** and **4**, respectively. This type of delocalization has also been observed in studies of the Fe(III)-containing, activated form of bleomycin,[49] an antibiotic that is activated by dioxygen,[50] and is a consequence of the π-donor properties of hydroxide and amide ligands. The wave function describing the five-coordinate Fe(III) intermediate **1** exhibits substantial spin polarization at its doublet-state geometry (Table S1), which appears to be primarily associated with unpaired spins located on the axial thiolate ligand (S3), although it is also evident that d orbitals, in addition to the d_{yz} orbital, possess some spin polarization. In combination with the insignificant energy difference computed between the "doublet" and "quartet" spin states of **1**, we conclude that the doublet ($S = {}^1/_2$) state is likely contaminated by the quartet ($S = {}^3/_2$) state in this calculation.

Structure and Bonding in the NHase Active-Site Model 1. An opportunity to evaluate the importance of including two conserved arginine residues on the β subunit of the

(44) This value corresponds to the dielectric constant of water at 20 °C, see: *Handbook of Chemistry and Physics*, 60th ed.; Weast, R. C., Ed.; CRC Press: Boca Raton, FL, 1979.
(45) Li, J.; Fisher, C. L.; Chen, J. L.; Bashford, D.; Noodleman, L. *Inorg. Chem.* **1996**, *35*, 4694−4702.
(46) Tissandier, M. D.; Cowen, K. A.; Feng, W. Y.; Gundlach, E.; Cohen, M. H.; Earhart, A. D.; Tuttle, T. R.; Coe, J. V. *J. Phys. Chem. A* **1998**, *102*, 7787−7794.
(47) Tawa, G. J.; Topol, I. A.; Burt, S. K.; Caldwell, R. A.; Rashin, A. A. *J. Chem. Phys.* **1998**, *109*, 4852−4863.
(48) (a) Figgis, B. N.; Hitchman, M. A. *Ligand Field Theory and Its Applications*; Wiley-VCH: New York, 2000. (b) Hitchman, M. A.; Riley, M. J. In *Inorganic Electronic Structure and Spectroscopy*; Solomon, E. I., Lever, A. B. P., Eds.; Wiley: New York, 1999; Vol. 1, pp 213−258. (c) Griffith, J. S.; Orgel, L. E. *Q. Rev.* **1958**, *11*, 381−393.
(49) Neese, F.; Zaleski, J. M.; Zaleski, K. L.; Solomon, E. I. *J. Am. Chem. Soc.* **2000**, *122*, 11703−11724.
(50) (a) Galm, U.; Hager, M. H.; Van Lanen, S. G.; Ju, J. H.; Thorson, J. S.; Shen, B. *Chem. Rev.* **2005**, *105*, 739−758. (b) Hecht, S. M. *J. Nat. Prod.* **2000**, *63*, 158−168. (c) Burger, R. M. *Chem. Rev.* **1998**, *98*, 1153−1169.

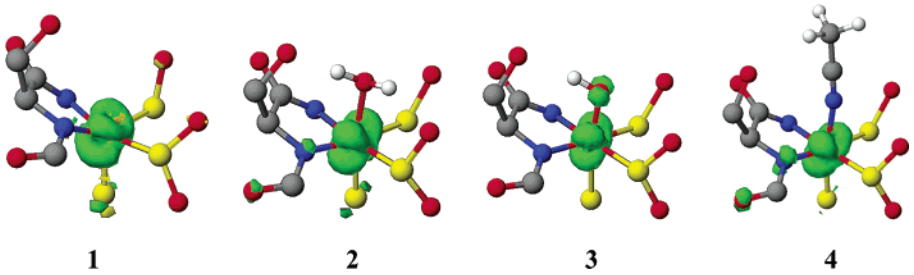

Figure 2. Close-up views of the spin magnetization density (SMD) computed from the B3LYP/6-31G* wave function for NHase active-site models **1**−**4** at their BLYP-optimized doublet geometries. Green and yellow isosurfaces, contoured at a value of 0.007 in all plots, show α and β densities, respectively. In the coordinate systems for these active-site models, the *z*-axis was placed along the Fe−S3 bond, with the *y*-axis being defined by one of the equatorial metal−sulfur (Fe−S1) bonds. For clarity, only non-hydrogen atoms are shown, which are colored using the following scheme: C, black; N, blue; O, red; S, yellow; Fe, red.

Table 1. Selected Structural Properties of the Initial and the BLYP-Optimized Doublet ($M_S = {}^1/_2$) Geometry for Active-Site Model **1**[a]

internal coordinate	initial structure[b,c]	$M_S = {}^1/_2$	$M_S = {}^1/_2$ (ref 50)
Fe−S1	2.33	2.33	2.37
Fe−S2	2.26	2.22	2.22
Fe−S3	2.30	2.20	2.20
Fe−N1	2.05	1.93	1.84
Fe−N2	2.09	1.91	1.88
S1−O2	1.51	1.63	1.69
S2−O3	1.51	1.54	1.69
S2−O4	1.41	1.58	1.48
O2−O3	3.37	3.25	2.99
O2−O5	5.56	4.75	5.28
O3−O5	5.43	5.39	4.52
S1−Fe−N2	171.1	153.3	164.9
S2−Fe−N1	175.6	162.1	152.6
Fe−S1−O2	107.8	103.4	105.6
Fe−S2−O3	115.6	113.8	100.7
O3−S2−O4	107.2	109.8	107.6
N1−S2−Fe−N2	1.1	−9.6	*d*
N2−S1−Fe−S2	2.2	−14.6	*d*

[a] Atom labels correspond to those shown in Figure 1. [b] Initial structures were constructed from the crystal structure of nitrosylated, Fe-type NHase, as described in the text. [c] All bond distances are reported in Å. Bond and dihedral angles are reported in degrees. [d] Data not reported in ref 51.

enzyme in our active-site models was provided by the availability of results from a prior computational study[51] of the five-coordinate Fe(III) intermediate formed when NO undergoes photodissociation from the inactive, nitrosylated enzyme. In this previous investigation, a smaller NHase active-site structure was optimized using a similar DFT model chemistry to the one described herein, in which the sulfenate and sulfinate oxygens were protonated in an effort to compensate for the absence of both arginine side chains. A comparison of the geometric parameters reported for this truncated model with those obtained for the larger NHase active-site model **1** after BLYP optimization showed that the two computed structures possessed similar geometrical properties (Table 1). For example, both calculations suggested that the metal in this coordinately unsaturated intermediate moves below the plane defined by the atoms in the four equatorial ligands. Perhaps more importantly, although the difference in protonation state of the sulfinate moiety in the two models does not affect the calculated Fe−S2 bond length (Table 1), the Fe−S1 bond in our optimized structure is 2.33 Å in length (identical to that observed in the crystal structure of inactive, nitrosylated NHase) rather than 2.37 Å, as reported in the earlier study.[51] In addition, our model predicts slighter longer Fe−N bond lengths, and the optimized S−O bonds of the cysteinyl ligands in the two models differ by as much as 0.15 Å in length. It is therefore uncertain whether merely protonating the sulfinate and sulfenate functional groups so as to decrease the computational requirements of the calculation is a good strategy, especially given the apparent importance of these arginine residues for catalytic activity.[52] Experimental validation of these computational observations on this transient intermediate awaits further spectroscopic studies on the photoactivated species formed by irradiation of the nitrosylated form of NHase.

Energetics and Structural Properties of NHase Active-Site Models 2−4 at their Spin-State-Dependent Optimized Geometries. Although the B3LYP vertical transition energies predict a low-spin ground state for active-site models **2**−**4**, we investigated whether this preference would persist on geometry optimization using the BLYP/6-31G* model chemistry at each of their three possible spin states. In addition, we were also interested in examining the impact of the Fe(III) spin state on the structural and bonding properties of active-site models **2**−**4**. Although well-converged geometries were obtained for **2** and **4** at all three possible spin states, this proved not to be possible for active-site model **3** in its sextet ($M_S = {}^5/_2$) state because of Fe−S bond dissociation during gas-phase optimization. We also observed that geometry optimization resulted in a proton transfer from the guanidinium moiety (corresponding to the side chain of Arg-56 in the β subunit) to the anionic oxygen of the sulfenate group in all three models. Although recent studies using Fourier transform infrared spectroscopy suggest that the sulfenate oxygen is not protonated in the enzyme at neutral pH,[53] we note that the guanidinium moiety continues to hydrogen bond to the neutral sulfenate, as observed in the crystal structure[10b] and, hence, conclude that this (possibly) artifactual proton transfer does not significantly affect the interpretation of these calculations. Importantly, the DFT wave functions obtained for the eight

(51) Nowak, W.; Ohtsuka, Y.; Hasegawa, J.; Nakatsuji, H. *Int. J. Quantum Chem.* **2002**, *90*, 1174−1187.

(52) Piersma, S. R.; Nojiri, M.; Tsujimura, M.; Noguchi, T.; Odaka, M.; Yohda, M.; Inoue, Y.; Endo, I. *J. Inorg. Biochem.* **2000**, *80*, 283−288.

(53) Noguchi, T.; Nojiri, M.; Takei, K.; Odaka, M.; Kamiya, N. *Biochemistry* **2003**, *42*, 11642−11650.

Table 2. Relative Energies and Noninteracting $\langle S^2\rangle_{KS}$ Values Calculated for the NHase Active-Site Models **2**−**4** at Their Spin-State-Dependent BLYP/6-31G*-Optimized Geometries

	BLYP/6-31G*			B3LYP/6-31G*		
active-site model	energy (cm^{-1})	$\langle S^2\rangle_{KS}$[a]	2S + 1	energy (cm^{-1})	$\langle S^2\rangle_{KS}$[a]	2S + 1
			2			
$M_S = {}^1/_2$	0	0.76	2.01	0	0.77	2.02
$M_S = {}^3/_2$	4060	3.80	4.02	1425	3.82	4.03
$M_S = {}^5/_2$	7195	8.76	6.00	1973	8.76	6.00
			3			
$M_S = {}^1/_2$	0	1.02	2.25	0	0.77	2.02
$M_S = {}^3/_2$	2247	3.80	4.02	10	3.82	4.02
$M_S = {}^5/_2$	*b*	*b*	*b*	*b*	*b*	*b*
			4			
$M_S = {}^1/_2$	0	0.76	2.01	0	0.77	2.02
$M_S = {}^3/_2$	3911	3.80	4.02	1032	3.82	4.03
$M_S = {}^5/_2$	7443	8.76	6.00	1744	8.76	6.00

[a] $2S + 1 = (4\langle S^2\rangle_{KS} + 1)^{1/2}$ (ref 74). [b] A fully converged structure could not be obtained due to dissociation of the Fe−S bonds during geometry optimization.

optimized structures exhibited minimal amounts of spin contamination, as measured by $\langle S^2\rangle_{KS}$ values (Table 2). Whereas active-site models **2** and **4** continued to prefer a doublet ($S = {}^1/_2$) ground state, the low- and intermediate-spin states computed for hydroxide-containing **3** differ in energy by only 10 cm^{-1}, representing an insignificant difference within the B3LYP/6-31G* formalism.[21i] This result, therefore, raises the possibility that if hydroxide were the sixth metal ligand in the resting enzyme, then one might expect both doublet and quartet spin states to be populated, which is not observed by EPR spectroscopy on the resting enzyme or during catalytic turnover.[4a] On the other hand, the small difference in the B3LYP/6-31G* energies computed for the optimized doublet and quartet structures may reflect the obvious limitations of in vacuo calculations.

We next investigated the spin-state-dependent electronic structure, structural properties, and chemical bonding in these BLYP-optimized Fe(III) active-site models. In NHase active-site model **2**, the metal−ligand bond lengths in the optimized structures generally increased on going from low- to high-spin states (Table 3). The Fe−S bonds exhibited the greatest dependence on spin state, with the largest effects being observed for the Fe−S2 bond (atom numbering as shown in Figure 1). As observed in previous calculations on peroxidases,[54] the Fe−O1 bond length in NHase active-site model **2** was greatest when the metal was in the quartet state. Perhaps the most notable spin-state-induced change in the geometry of active-site model **2** was its deviation from octahedral symmetry (Figure 3). For example, the low-spin structure exhibited slightly distorted octahedral coordination in which the equatorial ligands and the metal were essentially in the same plane and the O1−Fe−S3 angle was 168.1°. Changing the spin state, however, resulted in changes in the position of the sulfinate sulfur and amide nitrogens so that (i) the axial O1−Fe−S3 bond angle changed in increments of approximately 10° on going to the intermediate- and high-spin states and (ii) the metal moved below the plane defined by the equatorial ligands (Figure 3). The deviation from octahedral symmetry for the quartet spin-state is consistent with the need to break symmetry to obtain the intermediate-spin state. On the other hand, we anticipated a reduced electrostatic interaction between the water ligand and the Fe center in the sextet state. The deviation from octahedral symmetry for the model complex in the sextet state therefore appears to be a consequence of hydrogen-bonding interactions between water and the sulfinate oxygens and Ser-113 side chain (Figure 3).

Most of the optimized Fe−ligand bond lengths in NHase active-site model **3** increased in going from the doublet to the quartet, with the largest increase of 0.55 Å (Table 3) being observed in the bond between the metal and the sulfenate sulfur (Fe−S2) (atom numbering as shown in Figure 1). Although similar spin-state-dependent structural changes were observed in both **2** and **3**, such as the distortion of the octahedral coordination at higher spin multiplicities, the metal−hydroxide (Fe−O1) bond length was 0.24 Å shorter than the equivalent Fe−water bond in **2** at the doublet state (Table 2). In addition, the Fe−O1 bond in **3** did not lengthen significantly on going from the doublet to quartet spin state. Given these differences in the calculated Fe−O1 bond lengths for **2** and **3** at their low-spin states, we compared our results to experimental measurements on Fe-type NHase. In EXAFS studies performed prior to solution of the three-dimensional structure of the enzyme, the use of a 2S/3N/O coordination model gave predicted average Fe−S and Fe−N/O bond lengths of 2.208 and 2.000 Å, respectively, for the active form of the enzyme at a pH of 7.3.[55] These values compare to average Fe−N/O distances of 2.00 and 1.93 Å in our calculations on water-bound **2** and hydroxide-bound **3**, respectively. Equally, although both longer than those predicted from the EXAFS measurements, the calculated average Fe−S bond length for active-site model **2** (2.26 Å) is in better agreement with experiment than the value computed for **3** (2.36 Å). In an interesting observation, EXAFS studies of NHase at pH 9 supported a small increase in the Fe−N/O average distance (0.005 Å) and a decrease in the average Fe−S bond lengths (0.021 Å) about the metal center. One interpretation of these structural changes was that deprotonation of a metal-bound water molecule possessing a pK_a of approximately 8 took place on raising the solution pH. This explanation is not, however, consistent with these DFT calculations, which suggest that the average Fe−S bond length should *increase* upon deprotonation of the bound water, as might be expected from a competitive trans effect of the axial thiolate and hydroxide ligands. Unfortunately, superimposition of the optimized structures for **2** and **3** at their doublet ($S = {}^1/_2$) states onto the Fe(III) center seen in the 2.65 Å resolution crystal structure of the active form of NHase cannot be used to decide whether water rather than hydroxide anion is present in the sixth coordination site (Figure 4).

(54) Loew, G.; Dupuis, M. *J. Am. Chem. Soc.* **1997**, *119*, 9848−9851.

(55) Scarrow, R. C.; Brennan, B. A.; Cummings, J. G.; Jin, H.; Duong, D. J.; Kindt, J. T.; Nelson, M. J. *Biochemistry* **1996**, *35*, 10078−10088.

Table 3. Selected Structural Properties of the Initial and the Spin-State-Dependent DFT-Optimized Geometries for Active-Site Models **2**−**4**[a]

2 internal coordinate	initial[b,c]	$M_S = {}^1/_2$	$M_S = {}^3/_2$	$M_S = {}^5/_2$	**3** internal coordinate[d]	initial[b]	$M_S = {}^1/_2$	$M_S = {}^3/_2$	**4** internal coordinate	initial[b]	$M_S = {}^1/_2$	$M_S = {}^3/_2$	$M_S = {}^5/_2$
Fe−S1	2.32	2.36	2.41	2.71	Fe−S1	2.36	2.35	2.39	Fe−S1	2.36	2.36	2.40	2.64
Fe−S2	2.29	2.20	2.33	2.62	Fe−S2	2.20	2.28	2.83	Fe−S2	2.20	2.25	2.33	2.59
Fe−S3	2.33	2.23	2.43	2.39	Fe−S3	2.23	2.45	2.50	Fe−S3	2.23	2.26	2.40	2.37
Fe−N1	1.96	2.00	1.94	2.04	Fe−N1	2.00	2.00	2.09	Fe−N1	2.23	2.26	2.40	2.37
Fe−N2	1.95	1.92	1.93	1.98	Fe−N2	1.92	1.94	1.90	Fe−N2	1.92	1.92	1.94	1.98
Fe−O1	1.65	2.08	2.34	2.23	Fe−O1	2.08	1.84	1.82	Fe−N3	2.08	1.96	2.59	2.30
S1−O2	1.69	1.73	1.74	1.73	S1−O2	1.73	1.75	1.76	S1−O2	1.73	1.75	1.73	1.73
S2−O3	1.52	1.56	1.55	1.56	S2−O3	1.56	1.54	1.56	S2−O3	1.56	1.54	1.53	1.55
S2−O4	1.52	1.56	1.55	1.56	S2−O4	1.56	1.58	1.59	S2−O4	1.56	1.56	1.56	1.56
O1−O5	3.34	2.73	2.79	2.77	O1−O5	2.73	3.03	2.95	N3−O5	2.73		3.59	3.60
S1−Fe−N1	86.2	85.9	85.7	80.1	S1−Fe−N1	85.9	86.4	85.0	S1−Fe−N1	85.9	86.1	85.6	81.8
S1−Fe−N2	165.9	170.5	170.3	162.3	S1−Fe−N2	170.5	168.0	167.9	S1−Fe−N2	170.5	170.5	169.9	165.7
S2−Fe−N1	176.2	173.2	170.6	167.2	S2−Fe−N1	173.2	178.4	175.3	S1−Fe−N3	88.3	90.4	86.4	83.6
S2−Fe−N2	94.6	94.8	92.8	90.1	S2−Fe−N2	94.8	97.9	97.7	S2−Fe−N1	173.2	177.1	171.1	171.6
N1−Fe−N2	84.5	84.6	85.6	86.1	N1−Fe−N2	84.6	83.4	84.6	S2−Fe−N2	94.8	96.1	94.0	95.1
S2−Fe−S3	86.2	92.9	89.8	86.1	S2−Fe−S3	92.9	90.3	83.7	S2−Fe−N3	87.3	90.6	85.0	80.4
S1−Fe−O1	92.7	88.3	86.5	79.5	S1−Fe−O1	88.3	94.2	93.1	N1−Fe−N2	84.6	84.4	85.6	86.1
S2−Fe−O1	89.1	87.3	82.8	76.3	S2−Fe−O1	87.3	86.7	80.6	S2−Fe−S3	92.9	90.4	89.5	84.7
									Fe−N3−C1	180.0	170.5	148.7	153.9
									N3−C1−C2	180.0	176.6	177.9	177.6

[a] Atom labels correspond to those shown in Figure 1. [b] Initial structures were constructed from the crystal structure of nitrosylated, Fe-type NHase, as described in the Computational Methods section. [c] All bond distances are reported in Å. Bond and dihedral angles are reported in degrees. [d] Convergence of the geometry optimization could not be attained for this model structure at its sextet spin state.

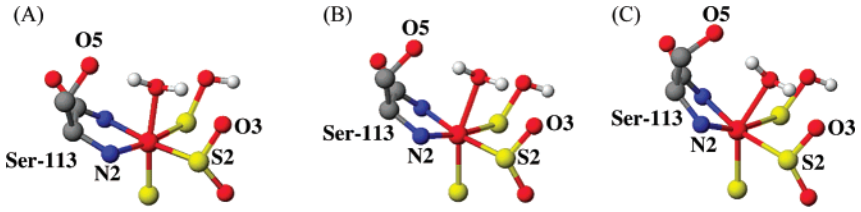

Figure 3. Optimized spin-state-dependent structures of the NHase active-site model **2**. (A) Doublet, (B) quartet, and (C) sextet. For clarity, only hydrogen atoms in important O−H bonds are shown. Atoms are colored using the following scheme: C, black; H, white; N, blue; O, red; S, yellow; Fe, red.

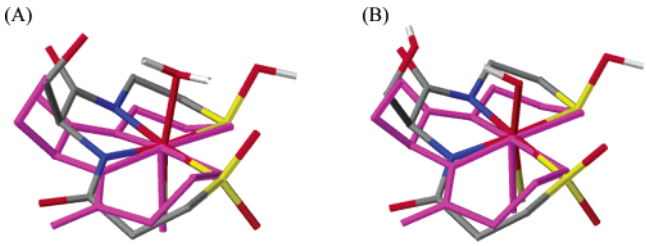

Figure 4. Superimposition of the metal center observed in the crystal structure of *Rhodococcus* R312 and the low-spin ($M_S = {}^1/_2$) DFT-optimized geometries of NHase active-site models **2** (left) and **3** (right). For clarity, only hydrogen atoms in important O−H bonds are shown. Atoms are colored using the following scheme: C, black; H, white; N, blue; O, red; S, yellow; Fe, red; crystal structure, purple.

The calculated Fe−S bond lengths exhibited the largest changes in the spin-state-dependent BLYP-optimized structures for active-site model **4** (Table 3). For example, the Fe−S1 and Fe−S2 bonds increased in length by 0.28 and 0.34 Å, respectively, on moving from a low- to a high-spin electronic configuration. A change of similar magnitude (0.34 Å) was also observed for the bond between the metal and the nitrile (Fe−N3), and there was a consistent decrease in the S3−Fe−N3 angle such that the nitrile bent toward the sulfinate moiety. Hence, the S3−Fe−N3 angle assumed values of 170.5°, 148.7°, and 153.9° for the low-, intermediate-, and high-spin states, respectively. In contrast, the Fe−S3 bond of the trans thiolate differed by only 0.11 Å in the doublet and sextet structures. Once again, these geometrical changes caused significant distortions in octahedral symmetry on moving from the low- to high-spin configuration, with the metal ion moving below the plane defined by the equatorial ligands.

Ground-State Electronic Structure of NHase Active-Site Models 2−4. A detailed analysis of the Kohn−Sham determinant describing each of the active-site models **2**−**4** at the doublet ($M_S = {}^1/_2$) state was performed both to (i) assess the quality of the DFT wave function and (ii) delineate the nature of the chemical bonding in these structures. The B3LYP first-order reduced density matrix was therefore obtained in an unrestricted formalism at the BLYP-optimized low-spin geometry and used to calculate NPA-derived partial charges and spin densities (Table 4). In all three NHase active-site models, the iron is positively charged and the amide nitrogens possess partial negative charges ranging from −0.59 to −0.63 |e⁻|. The reduction in formal Fe(III) charge can likely be attributed to the nephelauxetic effect, whereby ligand charge donation partially shields the metal d electrons from the central-ion nuclear charge and drives expansion of the d-electron "cloud".[56] The computed partial charges for the equatorial S ligands are also of comparable magnitude in all three models, the values of which range

(56) Schäffer, C. E. *Inorg. Chim. Acta* **2000**, *300*−*302*, 1035−1076.

Table 4. NPA-Derived Partial Charges and Spin Magnetization Densities (SMD) of Selected Atoms in NHase Active-Site Models **2**−**4** at Their BLYP-Optimized Doublet ($M_S = {}^1/_2$) Geometries[a]

2			**3**			**4**		
atom	partial charge	SMD	atom	partial charge	SMD	atom	partial charge	SMD
Fe	+0.47	+0.927	Fe	+0.60	+0.909	Fe	+0.41	+0.875
S1	+0.62	−0.020	S1	+0.59	−0.015	S1	+0.63	−0.019
S2	+1.69	−0.015	S2	+1.68	−0.012	S2	+1.70	−0.016
S3	−0.09	+0.085	S3	−0.36	+0.016	S3	−0.10	+0.084
N1	−0.63	−0.024	N1	−0.63	+0.017	N1	−0.63	+0.023
N2	−0.62	+0.042	N2	−0.62	+0.000	N2	−0.59	+0.078
O1	−0.95	+0.004	O1	−0.87	+0.133	N3	−0.38	+0.007
O2	−0.88	+0.004	O2	−0.88	−0.004	O2	−0.90	−0.008
O3	−1.03	−0.009	O3	−1.01	+0.006	O3	−1.02	−0.008
O4	−1.01	−0.008	O4	−1.03	−0.006	O4	−1.01	−0.007
O5	−0.79	+0.000	O5	−0.79	+0.000	O5	−0.81	+0.000
						C1	+0.47	+0.000
						C2	−0.79	+0.000

[a] Atom labels correspond to those shown in Figure 1.

from +0.59 to +0.63 $|e^-|$ and +1.68 to +1.70 $|e^-|$ for the sulfinate and sulfenate functional groups, respectively. Post-translational oxidation therefore serves to remove electron density from these sulfur ligands, in accord with chemical intuition. The nature of the ligand occupying the sixth coordination site about the metal, however, also has substantial effects on the partial negative charge of the axial thiolate. For example, when hydroxide anion is bound to the metal, as in active-site model **3**, the increased donation of electron density to the iron center by this σ/π donor increases the negative charge on the thiolate (S3) relative to its value in the other two models (Table 4). Once again, this observation is consistent with a competitive trans effect of the hydroxide and axial thiolate substituents. These NPA calculations also reveal the effects of coordinating water, hydroxide, or acetonitrile to the Fe(III) center of the enzyme. For example, when compared with the NPA charges on an unbound water molecule computed from a B3LYP single-point energy calculation, the partial charge on the ligand oxygen (O1) is basically unchanged by metal binding, being −0.93 and −0.95 $|e^-|$ for free and Fe-bound water, respectively. In the case of acetonitrile, NPA charges calculated from the B3LYP description of the free ligand are +0.28, −0.79, and −0.33 $|e^-|$ for C1, C2, and N3, respectively (atom numbering as shown in Figure 1). When the nitrile coordinates the Fe(III) center to yield **4**, however, C1 becomes more positively charged, as would be expected for a mechanism in which enzyme functions as a Lewis acid to increase the electrophilicity of the substrate. A more significant perturbation, however, is evident from studies of active-site model **3** in that the partial negative charge on the oxygen atom changes from −1.27 $|e^-|$ for free hydroxide to −0.87 $|e^-|$ for the bound ligand, which presumably reflects an increased charge transfer from O1 to the metal in **3** relative to that observed for **2**.

The calculated spin-magnetization densities for active-site models **2**−**4** are all consistent with those expected for a low-spin ($S = {}^1/_2$) d^5 system, with the excess α spin on Fe being within 0.125 units of the formal expectation value (Table 4). Visualization of the SMD reveals the extent to which spin is delocalized onto the metal ligands. For example, water binding, as in **2**, results in spin polarization on all of the ligands in the first coordination sphere, although the majority of α-spin delocalization is onto the axial thiolate (S3) and one of the amide nitrogens (N2). Evidence for the ionic character of the Fe−O1 bond in this active-site model, however, is provided by the observation that no significant spin delocalization onto the water oxygen is seen in these calculations. The SMD values computed for the acetonitrile-bound NHase model **4** are strikingly similar to those in the water-bound model, with the only significant difference being an increase in α-spin depolarization onto the N2 amide nitrogen. Replacing water by hydroxide anion, however, gives rise to extensive changes in the SMD of active-site model **3** compared with that of **2** (Table 4), of which the most notable is delocalization of the α spin onto the oxygen atom of bound hydroxide (O1). This effect can be rationalized on the basis of increased covalency in the bonding interaction between Fe and hydroxide. Such a hypothesis is also consistent with the increased partial negative charge of the trans thiolate ligand (S3) in this model, as discussed above. The reduced α-spin delocalization on one of the amide nitrogen ligands (N2) in **3** relative to its value in **2** also suggests increased ionic character in this metal−ligand interaction.

Ground-State Bonding in the NHase Active-Site Models 2−4. With access to the BLYP-optimized geometries and NPA-derived partial charges for the three active-site models, we undertook an analysis of NBO and NPA/NLMO bond orders together with comparisons of NBOs and their corresponding NLMOs to evaluate the contribution of σ overlap, π back-bonding, and π donation to metal−ligand bonding in these structures. This strategy of comparing NBOs with NLMOs to estimate the extent of covalency in metal−ligand bonding, particularly to distinguish σ- from π-symmetry interactions, is well precedented[57] and has been shown by our group to be an effective approach for describing chemical bonding in inorganic Fe(III) complexes with substantial N/S coordination.[22a] NBO bond orders in active-site models **2**−**4** were calculated using the following equation:

$$\sum (\mathrm{NBO_{BD}} - \mathrm{NBO_{BD^*}})/2$$

where $\mathrm{NBO_{BD}}$ and $\mathrm{NBO_{BD^*}}$ correspond to the occupancies of the bonding and antibonding NBOs, respectively. The first step in our analysis was to derive natural Lewis structures (NLSs) for **2**−**4** (Figure 5) by computing NBO-based values for the order (Table S2, Supporting Information) and the symmetry (Table S3, Supporting Information) of the chemical bonds. We note that NBOs, as linear combinations of one or two NHOs, yield an idealized picture of the optimal NLS for a given metal complex and a first approximation of the extent of covalency in metal−ligand bonding. Ionic bonds are defined to be those in which the relevant NBO was composed of greater than 95% of a single NHO. In agreement with the d^5 configuration for the metal, this

(57) Kaupp, M. *Chem.−Eur. J.* **1999**, *5*, 3631−3643.

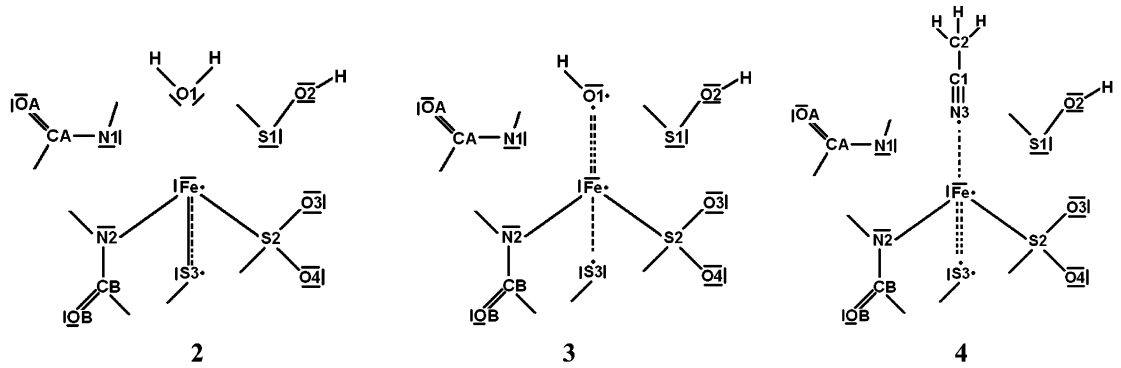

Figure 5. NBO-based idealized natural Lewis structures of NHase active-site models **2**−**4**. In these structures, NBOs containing a shared pair of α and β electrons are represented by solid lines, polarized one-electron bonds are shown as dotted lines, and dots correspond to unpaired electrons.

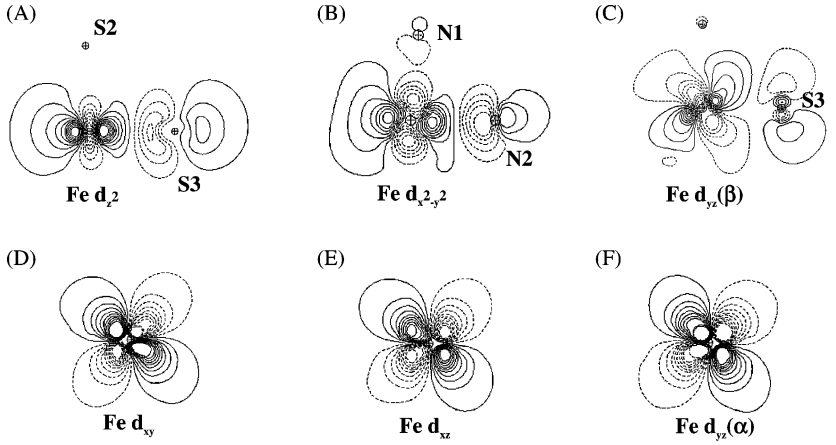

Figure 6. NBOs in NHase model **2** that possess significant Fe character. (A) Unoccupied e_g* Fe d_{z^2} NBO exhibiting strong antibonding character with S3. (B) Unoccupied e_g* Fe $d_{x^2-y^2}$ NBO. (C) Unoccupied t_{2g} Fe d_{yz} NBO. (D,E) d_{xy} and d_{xz} occupied t_{2g} Fe NBOs. (F) Singly occupied (α) t_{2g} Fe d_{yz} NBO. Atom labels indicate nuclei associated with the electrons in the MO and correspond to those shown in Figure 1. All contour plots were generated with *NBOView 1.0* using a value of 0.03.[75]

analysis showed that three occupied α and two occupied β NBOs were present on Fe in all three active-site models (Figure 6). These NBO calculations also indicated reduced covalent character in the Fe−N1 bonds of all three active-site models (Figure 5), supporting the hypothesis that the amide nitrogen (N1) is negatively charged. Support for this interpretation is provided by the presence of two lone pair (LP)[58] NBOs composed of NHOs that are linear combinations of mostly (>80%) degenerate p_z and p_x natural atomic orbitals (NAOs) on the nitrogen atom. In contrast, the Fe−N2 bond in all three NHase active-site models is sufficiently covalent to give rise to σ-type NBOs with calculated bond orders ranging from 0.75 to 0.78 (Table S2), although this bond is computed to be highly polar (<25% Fe character), being formed from a hybrid iron $sd_{x^2-y^2}$ NHO and a hybridized sp_y nitrogen NHO (Table S3). There is also a LP NBO located on N2, which is primarily composed of a p_z-character NHO.

The NBO-derived picture of the metal−sulfur bonding in active-site models **2**−**4** is, however, more complicated than that for the metal−nitrogen bonds. First, there is substantial variation in the Fe−S bonds within each of the three active-site models. The Fe−S1 bond is the least covalent of the three Fe−S bonds present in each individual model, and no two-center Fe−S1 NBO is evident in **2**−**4**. Two LP NBOs, of mostly 3s and p_y character, are therefore associated with S1. Given that the sulfenate oxygen is protonated in these gas-phase studies, however, there is the possibility that our calculations underestimate the extent of covalency in the Fe−S1 bond. In contrast, the chemical bond between the metal and the sulfinate sulfur atom (S2), in each of the NHase active-site models, involves a doubly occupied σ-type NBO formed by the combination of iron-$sd_{x^2-y^2}$ and sulfur-sp_x NHOs. No LP NBOs on S2 are evident in this computational analysis, and the occupancy of the S2−O3 and S2−O4 bonds suggests that these are best described as single bonds. As a result, each oxygen atom of the sulfinate moiety bears a negative partial charge (Table 4) because it possesses three LPs. This is further evidence for hydrogen bonding between the sulfinate oxygens and the adjacent arginine side chain in the β subunit. The observation that the nature of the Fe−S3 NBOs in the NHase active-site models **2**−**4** varies as a function of the ligand occupying the trans axial coordination site is, perhaps, the most important result of this analysis for the understanding of the catalytic mechanism. Hence, the Fe−S3 bond in **2** exhibits partial double-bond character because there is (i) a doubly occupied σ-type NBO formed

(58) As discussed more fully in ref 22a, although the NBO algorithm performs a separate analysis of the α and β spin-density matrixes, we (and the program authors) define a lone pair (LP) to signify a valence orbital localized essentially to a single atomic center despite the fact that this results in a maximum possible spin−orbital occupancy of 1.0.

between the iron sd_{z^2} NHO and a sulfur NHO possessing mostly p_z character and (ii) a singly occupied NBO of π-symmetry arising from S3 π donation into the Fe β d_{yz} NHO. The remaining valence electrons on S3 can then be associated with one doubly and one singly occupied LP NBO of predominantly s and p_y character, respectively. In the case of active-site model **4**, when acetonitrile is positioned trans to the axial thiolate, the Fe−S3 bond is formed by the overlap of Fe sd_{z^2} and d_{yz} NHOs with S3 p_z and p_y NHOs to form singly occupied σ- and π-symmetry bonds, respectively. There are, therefore, two singly occupied LPs on S3 composed of NHOs of mostly p_y and p_z character as well as one doubly occupied LP NBO of predominantly 3s character. The nature of the Fe−S3 bonding interaction is most perturbed, however, when water is replaced by hydroxide anion. In this case, the presence of hydroxide in the sixth coordination site reduces the covalency of the Fe−S3 bond such that the NBO is singly occupied and is formed from the σ-type overlap of Fe sd_{z^2} and S3 βp_z NHOs. Therefore, there is no π-symmetry interaction between the Fe and the axial thiolate group in this active-site model due to the presence of the competing π-donor hydroxide ligand.

The NBO-derived picture of the bonds between Fe and the exchangeable ligands in NHase active-site models **2**−**4** is also consistent with the expected binding properties of water, hydroxide, and acetonitrile. Hence, there is no formal NBO computed for the Fe−O1 bond in **2**, and only a small amount of σ-overlap of orbitals on the metal and acetonitrile nitrogen (N3) is observed in **4**. This is in support of the metal acting as a Lewis acid with no donation of metal electrons into the π^* orbitals of the nitrile group.[59] In contrast, hydroxide anion forms both σ- and π-symmetry metal−oxygen bonds in **3**. More specifically, two singly occupied NBOs are formed by the overlap of NHOs on Fe and O1 (Table S3), resulting in one doubly and two singly occupied LP NBOs on O1.

Our group has proposed, albeit on the basis of INDO/S-PUHF calculations, that deprotonated amide ligands in Fe(III) model complexes possess significant imidate character.[60] We therefore investigated whether these more accurate DFT calculations would support this hypothesis. At first glance, NBO analysis suggested that the carboxamido moieties in **2**−**4** might best be represented by amidate structures in which the negative charge was localized on nitrogen. Because NBO descriptions do not account for delocalization and the existence of alternate resonance forms, however, we also compared the localized NBOs with their corresponding NLMOs and NLMO/NPA bond orders (Table S4, Supporting Information). This comparison showed that neither resonance form of the deprotonated carboxamido ligands ($-N^{-}-C(R)=O$ and $-N=C(R)-O^{-}$) dominates in these active-site model structures, and hence, the deprotonated amides are best regarded as a "composite" in which the negative charge resides on both nitrogen and oxygen (Table S5, Supporting Information). In addition, three-center hyperbonds (3CHBs) (see below) involving all three atoms (N−C−O) in each amide are evident in these calculations, providing additional support for the existence of electron delocalization in these two metal ligands. It also appears that more imidate character is evident for the N1-containing amide (Figure 1), at least as judged from the calculated NLMO/NPA bond orders. The absence of any donor interaction from N1 to Fe to form a formal NBO in any of the active-site models **2**−**4** provides further support for this proposal. This bonding removes excess electron density from the nitrogen atoms coordinating the Fe(III) center, which thereby lessens the π-donor ability of the carboxamido moiety thus favoring a low-spin state for the metal.[5a,59]

Table 5. Covalent Character of Fe−Ligand Bonds in Active-Site Models **2**−**4** at Their BLYP-Optimized Doublet ($M_S = {}^1/_2$) Geometries[a]

bond	bond covalency ($\|e^-\|$) α spin	bond covalency ($\|e^-\|$) β spin	$\alpha + \beta$ ($\|e^-\|$)	total covalency ($\|e^-\|$)
		2		
Fe−S1	0.133	0.125	0.258	2.053
Fe−S2	0.179	0.170	0.349	
Fe−S3	0.295	0.367	0.661	
Fe−N1	0.141	0.124	0.265	
Fe−N2	0.192	0.247	0.439	
Fe−O1	0.009	0.073	0.081	
		3		
Fe−S1	0.119	0.116	0.236	2.004
Fe−S2	0.156	0.150	0.306	
Fe−S3	0.122	0.155	0.278	
Fe−N1	0.133	0.125	0.258	
Fe−N2	0.188	0.198	0.386	
Fe−O1	0.219	0.323	0.542	
		4		
Fe−S1	0.133	0.125	0.258	2.152
Fe−S2	0.178	0.174	0.352	
Fe−S3	0.276	0.331	0.607	
Fe−N1	0.140	0.122	0.262	
Fe−N2	0.191	0.286	0.477	
Fe−N3	0.080	0.115	0.195	

[a] Atom labels correspond to those shown in Figure 1.

Having derived this qualitative picture of Fe-ligand bonding in the three model structures, we next examined the extent of bond covalency using methodology that we have calibrated in theoretical studies of iron−nitrosyl complexes (Table 5).[13a] In this approach, the comparison of NLMOs with their corresponding NBOs permits classification of electron delocalization into such categories as σ donation, π back-bonding, and π donation. The detailed comparison of calculated covalency with the NBO-derived bond orders also provides information on the strength of the acceptor−donor interaction in a given Fe−ligand bond, because it captures effects from electron delocalization that are evident in the NLMOs as well as in NBO composition. For example, a completely covalent Fe−ligand bond would give rise to an NBO composed equally of NHOs from iron and its coordinating atom. In obtaining bond covalencies, however, we also consider 3CHBs,[22a] which most commonly arise from the interaction of a LP on one atom with the formal NBO between two other atoms. The calculated bond covalencies and symmetries of the $Fe-N_{amide}$ bonds in the active-site models clearly show the influence of the unsymmetrical

(59) Zanella, A. W.; Ford, P. C. *Inorg. Chem.* **1975**, *14*, 42−47.
(60) Boone, A. J.; Cory, M. G.; Scott, M. J.; Zerner, M. C.; Richards, N. G. J. *Inorg. Chem.* **2001**, *40*, 1837−1845.

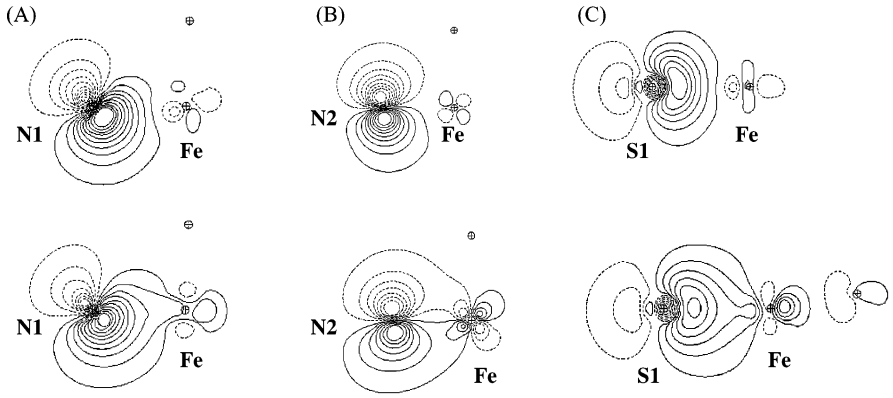

Figure 7. NBO (top) and corresponding NLMO (bottom) representations of Fe−ligand bonding in NHase active-site models. (A) Ligand-to-metal σ donation from N1 to Fe. (B) Ligand to metal π donation from N2 to Fe. (C) ligand-to-metal σ donation from S1 to Fe. Atom labels, which indicate the nuclei associated with the electrons in the MO, correspond to those shown in Figure 1, and all contour plots were generated using *NBOView 1.0* using a value of 0.03.[75]

environment upon the ability of the deprotonated amides to form bonds to the iron center. For example, our analysis of electron delocalization shows that the Fe−N1 bonds in active-site models **2**−**4** possess some covalent character, with calculated values ranging from 0.258 to 0.265 |e$^-$| (Table 5). The importance of including such delocalization effects is emphasized by the fact that no formal NBO between the metal and N1 is present in the NLS of any of these active-site models (Figure 5). The covalency in the Fe−N1 interaction seems to be primarily associated with ligand-to-metal σ donation of electrons from the N1 LP NBOs into the Fe−S2 NBO, thereby forming a 3CHB that is evident by comparing the LP NBO and LP NLMO on nitrogen N1 (Figure 7A). Even though the LP NBOs on N1 donate electron density into the metal center, a more significant fraction of the electron density is delocalized over the amidate atoms (N1−CA−OA). The covalency calculated for the bond between the metal and the other carboxamido ligand (Fe−N2) is less than expected from the NBO-derived bond order, although it still exceeds that of the Fe−N1 bond. This situation arises because the Fe−N2 NBO is composed of only 11.6−24.8% of the NHO on the metal; thus, this bond has significant ionic character. We also note that N2 participates in a 3CHB via π donation of the p_z LP into the Fe−S3 NBO of π-symmetry in NHase active-site models **2** and **4** (Figure 7B). There is considerable covalency in the Fe−S1 bond in all three active-site models, apparently reflecting formation of a 3CHB that involves ligand-to-metal σ donation from the S1 p_y LP into the Fe−N2 NBO (Figure 7C). On the other hand, the covalency calculated for the Fe−S2 bond in **2**−**4** is less than expected given the magnitude of the NBO-based bond order, primarily because the electrons are shared unequally so that the metal contributes only about 20% of the NHOs. Although sulfur is considered to be a strong π-donor, no such interactions are observed for either of the oxidized sulfur ligands (S1 and S2) in the active-site models, and the nature of the metal−ligand interactions involving the sulfenate and sulfinate moieties is complicated by a number of competing effects.[61] For example, the loss of filled π-symmetry LPs on sulfur upon oxidation decreases $d_\pi-p_\pi$ repulsion between these LPs and the filled t_{2g} orbitals on the metal (increasing the Fe−S bond order), even as the oxygen atoms lower the σ-donor ability of the sulfur ligands thereby weakening the strength of the Fe−S interaction. As a result, in active-site models **2** and **4**, which share many similar bonding features, the covalencies calculated for the Fe−S1 and Fe−S2 bonds are lower than those for the thiolate ligand (S3), suggesting that the loss of σ-donor ability has a larger effect than the loss of $d_\pi-p_\pi$ repulsion. Even though the Fe−S3 bond in these two active-site models has the highest amount of calculated covalency, this is not the case for **3** because the hydroxide anion, a superior π-donating ligand, competes with S3 to form a π-bond with the Fe d_{yz} as well as a σ-bond due to its interaction with the Fe d_{z^2} orbital (Table 5).

There is no appreciable covalency calculated for the Fe−O1 bond in the active-site model **2** when water occupies the sixth coordination site about the metal. This is not the case, however, for the ligands in **3** and **4**, where an electron in a ligand p_z orbital participates in significant three-center hyperbonding with the trans thiolate. More specifically, when hydroxide is bound to the metal (**3**), there is σ donation from the α p_z LP orbital on S3 into the Fe−O1 σ-bond as well as σ donation of a β electron from O1 into the Fe−S3 σ-bond, reflecting the similar σ-donor strengths of the hydroxide and thiolate ligands. The Fe−O1 bond in **3** therefore exhibits more covalency than the cognate bond in active-site model **2**, but its ionic character is reflected in the fact that the calculated covalency (Table 5) is less than expected from consideration of the NBO bond order (Table S2). The Fe−N3 bond in **4**, when acetonitrile occupies the sixth coordination site, is formed predominantly by σ donation of the N3 LP into the Fe center and has a calculated covalency that lies between those computed for the Fe−O1 bonds in **2** and **3** (Table 5). In part, this reflects the effect of a 3CHB interaction associated with σ donation from the N3 LP NBO

(61) (a) Grapperhaus, C. A.; Darensbourg, M. Y. *Acc. Chem. Res.* **1998**, *31*, 451−459. (b) Ashby, M. T.; Enemark, J. H.; Lichtenberger, D. L. *Inorg. Chem.* **1988**, *27*, 191−197.

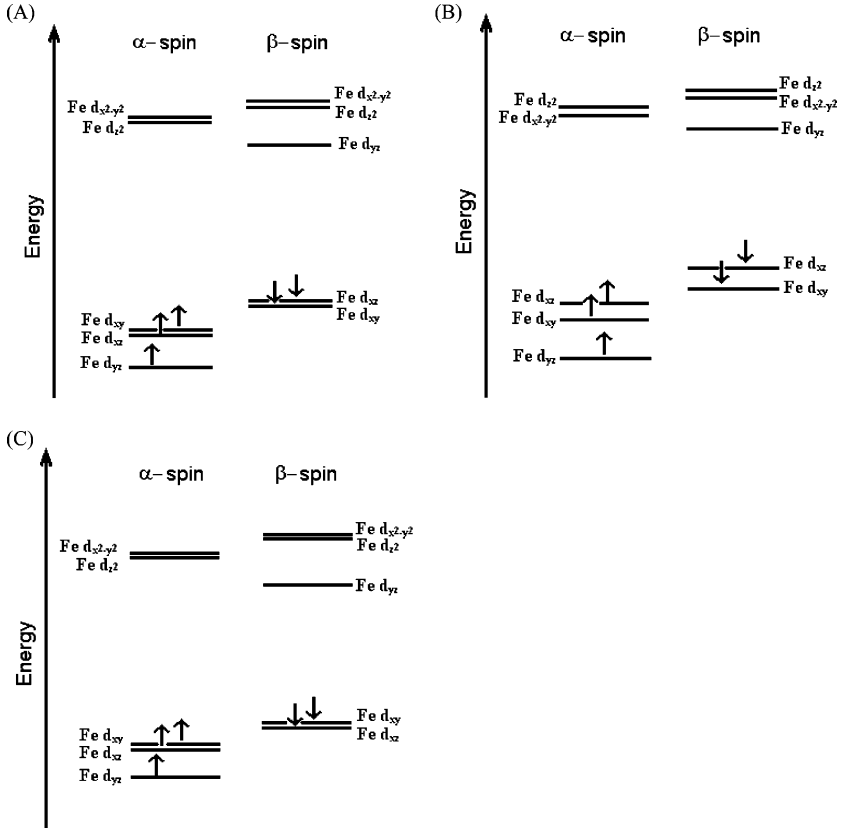

Figure 8. Qualitative diagrams of the iron-based molecular orbital energies in the NHase active-site models. (A) **2**; (B) **3**; (C) **4**.

into the trans Fe−S3 bond, similar to that observed in active-site model **3** (see above). On the other hand, when water is bound to the metal, the observed three-center hyperbonding involves only S2−Fe−N1, N2−Fe−S1, and S3−Fe−N2 interactions. The latter 3CHB between the axial thiolate and the nitrogen (N2) of a deprotonated amide is not present, however, when hydroxide replaces water, because S3 now interacts strongly with the Fe−O1 bond.

This NBO description of the chemical bonding in these active-site models provides an opportunity to determine how the unusual N/S ligand field in the non-heme Fe(III) center might give rise to the orbital splitting that results in the low-spin preference observed for NHase.[4a] First, although deprotonated amides were shown to be the strongest π-donors in recent computational studies on activated bleomycin,[49] the imidate character of these moieties in NHase results in Fe−amide bonds that are formed primarily by σ donation into the Fe $d_{x^2-y^2}$ orbital. The σ-donor properties of carboxamido nitrogens have been discussed elsewhere.[15l] As a result, the ligand-field splitting is increased because stabilization of the bonding e_g MO raises the energy of the corresponding, unoccupied antibonding e_g* MO (formed from Fe $d_{x^2-y^2}$) into which electrons must be placed to form a higher spin state (Figure 8A). In addition, π donation from the amide nitrogens, which is substantially reduced due to the contribution of the imidate resonance structure, is mostly into the Fe−S antibonding orbitals and, therefore, has a minimal effect on the energy of the d_{xy} and d_{yz} orbitals. The orientation of the equatorial sulfur ligands, in combination with oxidation of S1 and S2 (Figure 1), also modulates the donor interactions of these atoms with the metal center. Thus, thiolates are generally considered as weak field ligands given their ability as π-donors, but in all three NHase active-site models, oxidation of the equatorial sulfur ligands effectively abolishes their π-donor capability, ensuring that their interaction with the Fe(III) center is restricted to σ donation into the $d_{x^2-y^2}$ orbital. This again acts to increase the energetic separation of the t_{2g} and e_g* orbitals, favoring a doublet spin state. An additional destabilization of the $d_{x^2-y^2}$ e_g* orbital may also result from the 3CHB interactions involving the sulfur ligands and the amide Fe−N bonds, which act to decrease pairing energy in the $d_{x^2-y^2}$ orbital because of the nephelauxetic effect. This NBO analysis also suggests that the axial thiolate in **2** and **4** plays a critical role in determining the nature of the singly occupied MO (SOMO) on the metal center, not only through π donation into the Fe d_{yz} orbital but also by destabilizing the Fe d_{z^2} e_g* orbital via a σ-symmetry interaction with the metal. Because the axial thiolate destabilizes the d_{z^2} orbital and the equatorial ligands destabilize the $d_{x^2-y^2}$ orbital in these two active-site models, the energetic splitting between the e_g* orbitals is small (Figure 8). In contrast, for **3**, in which both axial ligands make significant σ-donor interactions with Fe, we find that the d_{z^2} orbital is higher in energy than the $d_{x^2-y^2}$ orbital (Figure 8B); this order is inverted when compared with those of **2** and **4**. In a finding that is consistent with recent studies of an inorganic Fe(III) complex prepared as a model for the NHase

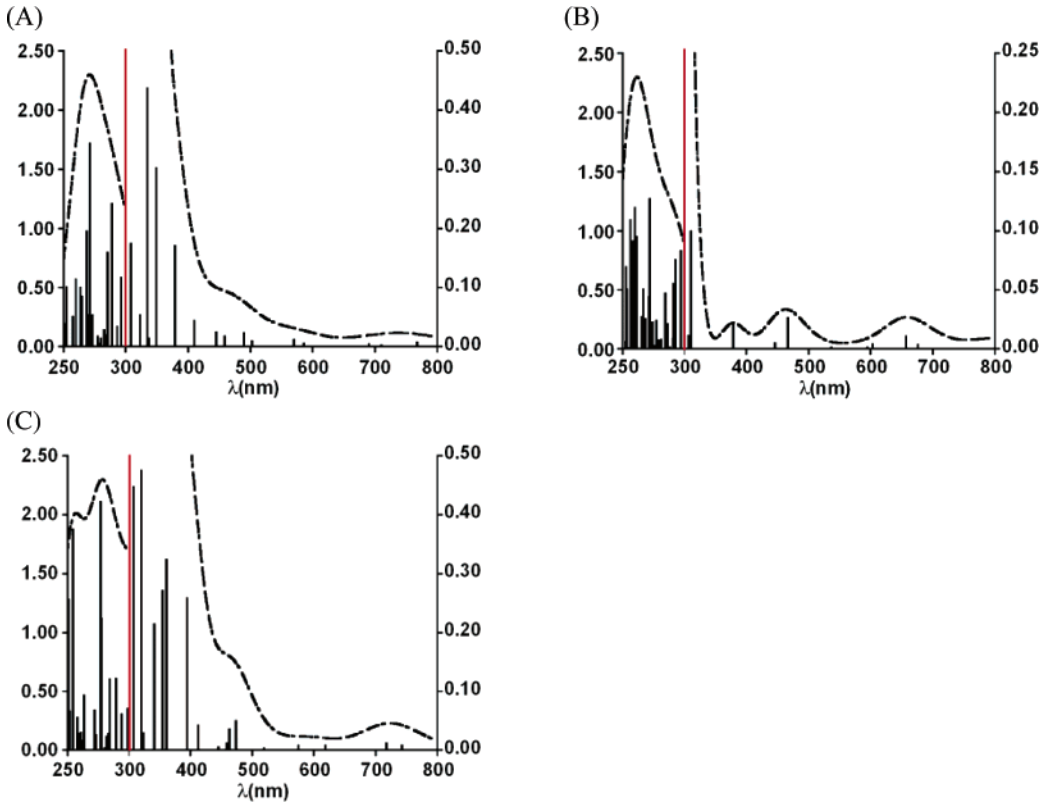

Figure 9. Simulated UV-visible spectra of active-site models **2**−**4** at their BLYP-optimized geometries. In all simulated spectra, vertical lines show the theoretical absorption maxima, and their length is proportional to calculated INDO/S CIS oscillator strength. The dashed lines represent a fit to Gaussian functions with bandwidths of 3200 cm^{-1}, normalized to the height of the highest-energy transition. The red vertical line in each figure shows a change in absorption scale. In vacuo INDO/S CIS spectra calculated for (A) **2**, (B) **3**, and (C) **4**.

metal center,[62] we find that the strong π-donor axial thiolate and hydroxide ligands dominate the t_{2g} orbital splitting pattern and the nature of the SOMO in these active-site models. For example, the computed orientation of hydroxide in **3** permits unbalanced π donation into both the Fe d_{yz} and d_{xz}, resulting in an axial distortion of all the t_{2g} orbitals. In contrast, there is no appreciable axial splitting of the Fe d_{xz} and d_{xy} orbitals in **2** and **4**, which are both effectively nonbonding with respect to the ligands.

Calculated UV−Visible Spectroscopy of NHase Active-Site Models 2−4. The in vacuo spectroscopic properties of the lowest-energy, BLYP-optimized structures for active-site models **2**−**4** were computed by INDO/S CI singles (CIS) calculation,[38] and compared to those of experimental spectra obtained for active NHase undergoing steady-state turnover.[9b,16,63] The enzyme exhibits absorption maxima at 676 and 280 nm, as well as two shoulders at 370 and 450 nm, in the presence of substrate. It is important to note that this spectrum corresponds to that obtained for NHase when *n*-butyric acid is absent during purification. This choice, therefore, avoids possible complications due to coordination of the Fe(III) center by the short-chain fatty acid at neutral pH, although such an interaction has only been observed definitively for the Co-containing form of the enzyme.[2f] Not only do such theoretical studies of molecular spectroscopy permit the evaluation of the quality of the optimized model structures, but they also have the potential to identify the nature of the species that are present at significant concentrations in the conditions used for the experimental measurements. On this point, we were particularly interested in establishing whether the sixth metal ligand in the free enzyme was water or hydroxide, given that most mechanistic proposals assume that Fe-bound hydroxide participates in catalysis.[2,3,5,6,10] On the other hand, any comparison of experimental and theoretical findings is complicated by the absence of systematic studies about the dependence of the UV−visible spectroscopy upon reaction conditions, and few details have been provided concerning the conditions under which known spectra have been determined.[9b,16,63]

For calculations on active-site model **2**, the CI included all possible single excitations from the 30 occupied MOs of highest energy into the 20 lowest-energy unoccupied MOs. The theoretical electronic spectrum exhibited one weak absorption maximum at 737 nm, a strong absorption at 270 nm, and a shoulder at approximately 465 nm (Figure 9A). The experimental and theoretical spectra are in remarkable agreement, with differences of 1224, 717, and 1323 cm^{-1} for the absorption features at 737, 465, and 270 nm, respectively, although a shoulder observed experimentally at 370 nm was absent from the calculated spectrum. Nevertheless, and especially because two absorption features with large oscillator strengths are present at 350 and 380

(62) Kennepohl, P.; Neese, F.; Schweitzer, D.; Jackson, H. L.; Kovacs, J. A.; Solomon, E. I. *Inorg. Chem.* **2005**, *44*, 1826−1836.
(63) Nagamune, T.; Kurata, H.; Hirata, M.; Honda, J.; Koike, H.; Ikeuchi, M.; Inoue, Y.; Hirata, A.; Endo, I. *Biochem. Biophys. Res. Commun.* **1990**, *168*, 437−442.

nm, our results permit a preliminary assignment of the electronic transitions computed for NHase active-site model **2** (Table S6, Supporting Information). In the INDO/S model chemistry, the highest-energy occupied MOs were principally composed of ligand nonbonding orbitals, with near degeneracy of the trans thiolate S3$_\pi$ and the amide N2$_\pi$ orbital. The INDO/S wave function identified the Fe d_{yz} orbital as the ROHF SOMO, in agreement with the results of the NBO analysis performed using the Kohn−Sham orbitals (see above).[64] Although a π* orbital localized on the guanidinium group modeling the β-Arg-151 side chain was computed to be the LUMO, the next highest-energy orbitals (LUMO+1 and LUMO+2) corresponded to the Fe−ligand σ-antibonding e_g* MOs. Given their small energetic separation, there is significant mixing of these two ROHF e_g* MOs, reflecting the similar σ-donor strengths of the axial thiolate and the equatorial carboxamido ligands. Thus, the MO-based INDO/S model again shows agreement with our NBO-based interpretation of the Kohn−Sham orbitals describing this active-site structure (see above). Two electronic $d_\pi \rightarrow d_\pi$ transitions, associated with promotion of an electron from the Fe d_{xy} and d_{xz} MOs into the singly occupied Fe d_{yz} MO (Figure S2, Supporting Information), had calculated absorption energies of less than 5000 cm^{-1}. These low-energy transitions therefore appear to reflect the strength of the π-symmetry interaction between the axial thiolate ligand and the SOMO located primarily on Fe(III). We note that this interpretation is consistent with experimental findings obtained in magnetic circular dichroism (MCD) studies[62] of an inorganic Fe(III) complex that was prepared specifically as a model for the metal center in NHase.[5,15o,p] The broad, low-energy absorption peak at 737 nm in the theoretical spectrum is composed of three transitions located at 768 nm (13 021 cm^{-1}), 710 nm (14 085 cm^{-1}), and 690 nm (14 493 cm^{-1}), which can all be assigned primarily to be $d_\pi \rightarrow d_\sigma$ in nature, whereas the 690 nm absorption feature arises from promotion of an electron from the SOMO d_{yz} into an MO composed primarily of the Fe d_{z^2} orbital. At first sight, the latter finding contradicts results from resonance Raman spectroscopy that have been interpreted as showing the low-energy absorption peak in resting NHase arises from a S → Fe CT transition.[17] This disagreement might, however, be explained by considering two points. First, all three of the calculated low-energy transitions involve some contribution from excitations of ligand-to-metal charge transfer (LMCT) character involving electrons on the sulfinate oxygens and the Fe−N1 σ-bond (Table S6). In addition, the transitions that make up the low-energy absorption peak are calculated to involve MOs that are strongly antibonding with respect to the Fe−S bonds. As a result, promotion of an electron into either of the e_g* MOs might be expected to perturb metal−ligand stretching modes, consistent with the resonance Raman observations. The shoulder at 465 nm in the theoretical spectrum of **2** is also composed of three transitions centered at 490 nm (20 408 cm^{-1}), 459 nm (21 786 cm^{-1}), and 445 nm (22 472 cm^{-1}) (Table S6). We assign the absorption feature at 490 nm to be an LMCT-type excitation in which the electron is promoted from an LP orbital on one of the deprotonated amides into the iron e_g* MOs. There also appears to be an energetically degenerate $t_{2g} \rightarrow e_g$ transition at 490 nm. The remaining higher-energy, $d_\pi \rightarrow d_\sigma$ transitions are relatively weak in nature and are coupled to CT excitations involving Fe−ligand MOs (Figure S2). Transitions of energy greater than 23 000 cm^{-1} in these INDO/S CIS calculations mostly arise from LMCT or involve MOs centered on the ligand. Of the former, ranging from approximately 310−380 nm (32 258−26 316 cm^{-1}), the electron is promoted from the S3$_\pi$ and/or LP orbitals in one of the deprotonated amides into the SOMO and e_g* MOs on Fe. There is also an absorption feature calculated at 285 nm, which is associated with two nearly degenerate transitions, the first being an $n \rightarrow \pi$* transition in "amide 2" (Figure S2) and the second corresponding to an electronic promotion from the S3$_\pi$ and the N2 and OB (Figure 5) LPs into the Fe d_{yz} MO. A similar transition of a LP electron on the other deprotonated amide ligand into the SOMO on the metal is also observed at a slightly lower wavelength of 273 nm. This electronic transition is also coupled to charge transfer from the thiolate sulfur (S3). The final two high-energy absorption features in the calculated spectrum can be assigned as LMCT transitions from the nonbonding LPs on the amide oxygen atoms into the Fe 3d_σ MOs.

The UV−visible transitions computed for NHase active-site model **3** (Figure 9B) also compared reasonably well to those seen in the experimental spectrum of the resting enzyme, with the absorption peaks calculated at 660 nm (15 151 cm^{-1}), 467 nm (21 413 cm^{-1}), 378 nm (26 455 cm^{-1}), and 260 nm (38 461 cm^{-1}), corresponding to the experimental absorption features at 676, 450, 370, and 280 nm, with errors of 358 , 809, 572, and 2747 cm^{-1}, respectively (Table S7). As observed for NHase active-site model **2**, the weak, low-energy transitions calculated for **3** correspond mostly to ligand-field transitions coupled to charge-transfer transitions. In this complex, however, the e_g* MOs are not energetically degenerate because the 3d_{z^2} orbital is higher in energy than the $d_{x^2-y^2}$ orbital due to stronger σ interactions between the axial hydroxide and thiolate ligands than between the equatorial ligands and the Fe $d_{x^2-y^2}$ orbital. In addition, both the d_{xz} or d_{yz} orbitals in the INDO/S ROHF wave function are rotated by approximately 45° from the metal−ligand bonds (Figure S3, Supporting Information) because of the symmetry of the π interaction between orbitals on the hydroxide oxygen (O1) and iron. This appears to be the result of hydrogen bonding between the Ser-113 side chain and the metal-bound hydroxide. Once again, there is agreement between the NBO analysis based on Kohn−Sham MOs and the INDO/S ROHF orbitals in that the LPs on the sulfinate and sulfenate moieties (O3 and O4) are degenerate and nonbonding with respect to the Fe d_{xy} orbital. Therefore,

(64) In previous EPR studies on resting NHase, it was suggested that the unpaired electron is located in the d_{xy} orbital. This assignment, however, was based on an analysis that assumed the absence of covalency in the metal−ligand bonds. In addition, insufficient details were given regarding the choice of coordinate system for the proposed model of the Fe site structure. Given that the d_{xy} and d_{yz} orbitals are both in the t_{2g} set, however, it is likely that the difference between the computational and theoretical assignments has no physical significance.

transitions from Fe d_{xy}, such as that seen at 812 nm (12 315 cm^{-1}) for which the electron is promoted into an MO comprised primarily of Fe $d_{x^2-y^2}$, are coupled with charge transfer from O3 and O4. Other calculated low-energy absorption features are assigned as $d_\pi \rightarrow Zd_\pi$ transitions into the singly occupied Fe d_{yz} MO (SOMO). The absorption at 660 nm is comprised of two transitions located at 676 nm (14 792 cm^{-1}) and 657 nm (15 220 cm^{-1}), which are both $t_{2g} \rightarrow e_g$ transitions from the d_{yz} MO into the d_{z^2} and $d_{x^2-y^2}$ MOs, and the calculated absorption peaks at 467 and 378 nm are assigned as ligand-field transitions from the d_{yz} and d_{xy} MOs into the d_σ iron MOs (Table S7). In contrast to our results for the water-bound **2**, the relative magnitudes of the oscillator strengths calculated using **3** do not match the observed absorptivities for the corresponding features in the experimental UV/visible spectrum of resting NHase at neutral pH. Higher-energy absorption features can all be assigned as ligand−metal charge transfer (LMCT) transitions, primarily involving the π-symmetry MOs on the two deprotonated amides and the thiolate sulfur (S3) (Table S7). For example, the three calculated electronic transitions at 261 nm (38 314 cm^{-1}), 260 nm (38 461 cm^{-1}), and 258 nm (38 759 cm^{-1}), which together make up the absorption peak centered on 260 nm, arise from an $S3_\pi \rightarrow$ Z Fe $3d_{z^2}$ CT transition, the promotion of an electron from the nitrogen and oxygen LPs on amides **1** and **2** into the Fe $3d_{z^2}$ MO, and from the $S3_\pi$ orbital into the Fe d_{yz} SOMO, respectively. In addition, other high-energy transitions appear to be associated with electron transfer from LPs on the carboxamido ligands into the Fe SOMO and d_σ orbitals.

Although it has not been unambiguously demonstrated that nitriles bind directly to the Fe(III) center of NHase,[65] spectroscopic studies of solutions containing active NHase, albeit in the presence of *n*-butyric acid, have shown that the addition of propionitrile blue-shifts the low-energy absorption peak observed for the enzyme by about 500 cm^{-1}, from 712 to 690 nm.[4a] It is therefore interesting that this shift is reproduced in the calculated INDO/S CIS spectra of active-site models **2** (Figure 9A) and **4** (Figure 9C). Thus, the low-energy peak in the acetonitrile-bound complex **4** is centered at 719 nm (13 908 cm^{-1}) (Table S8, Supporting Information), whereas the cognate absorption in **2** is calculated to be at 737 nm (13 568 cm^{-1}) (Table S6), equivalent to a blue-shift of 340 cm^{-1}. Although we recognize that this energy difference lies within the error of the INDO/S CIS method,[38] we note that when hydroxide occupies the sixth coordination site, the low-energy absorption calculated for **3** is red-shifted by 1244 cm^{-1} to 660 nm. This is contrary to experimental observations and provides additional support for a model of the resting enzyme in which water is bound to the Fe(III) center. Once again, INDO/S ROHF MOs are identical to those obtained from NBO analysis of the Kohn−Sham orbitals representing the B3LYP wave function, with the e_g* MOs being almost identical in energy. As for **2**, this likely reflects the similar σ-donor ability of the axial and equatorial ligands. As might be expected from our NBO analysis, the t_{2g} MOs are also strikingly similar to those of the H_2O-containing NHase model, with the unpaired electron being located in the Fe d_{yz} orbital (Figure S4, Supporting Information). The absorption maximum computed at 719 nm for **4** appears to comprise two $d_\pi \rightarrow d_\sigma$ transitions (Table S8). The first of these is a transition from the Fe d_{xy} orbital into the e_g* MOs, and the second can be assigned as a $d_{yz} \rightarrow d_{z^2}$ transition. Additional calculated absorption maxima for active-site model **4** are centered at 470 nm (21 276 cm^{-1}), 350 nm (28 571 cm^{-1}), and 278 nm (35 971 cm^{-1}) (Figure 9C). The absorption maximum at 470 nm can attributed to two absorption features at 474 and 463 nm, which are assigned as an SOMO $\rightarrow d_{x^2-y^2}$ transition, and an LMCT transition from the nearly degenerate N1 and S3 p MOs into the Fe d_{z^2} orbital, respectively (Table S8). Higher-energy absorption features mostly arise from LMCT transitions. For example, the calculated absorptions at 362 nm (27 624 cm^{-1}), 355 nm (28 169 cm^{-1}), and 341 nm (29 325 cm^{-1}) all originate by promotion of an electron from orbitals of π-symmetry on the amide nitrogens and the axial thiolate ligand (S3) into the Fe d_{z^2} and d_{yz} MOs. The absorption maximum centered at 278 nm can also be assigned as a transition from the N1 and S3 π orbitals into the Fe $d_{x^2-y^2}$ MO. Finally, the absorption calculated at approximately 255 nm arises by electronic promotion from nonbonding LPs on the amide oxygens into the Fe SOMO and e_g* MOs (Table S8).

Ligand-Exchange Energetics. The structural and spectroscopic features calculated for active-site model **2**, in which water is bound in the sixth coordination site, are more consistent with the physical properties of resting NHase than those computed for **3**. We therefore undertook a systematic evaluation of the energies for replacing water or hydroxide anion by acetonitrile (Scheme 1). Because the B3LYP DFT self-interaction energy of free hydroxide precludes accurate results for isodesmic reactions involving this species,[66] we decided to obtain the ligand-exchange energy for the conversion of **3** to **4** using a thermodynamic cycle relating the three active-site models (Scheme 1). This strategy required only the energy of the isodesmic reaction involving active-site model **2** and acetonitrile to form **4** and water (Scheme 2A) to be obtained by DFT calculations. The effects of the protein environment and moving acetonitrile out of, and water into, aqueous solution were modeled by SCRF methods and the appropriate choices of the dielectric constant (20 and 80.37 for the protein and aqueous environment, respectively).[42] Using gas-phase B3LYP/LACV3P++ energies, zero-point energy and thermal corrections, and solvation free energies in the appropriate thermodynamic cycle (Scheme 2B) gave a value of $\Delta G = +7.2$ kcal/mol for the substitution of Fe-bound water by acetonitrile (Table S9, Supporting Information). Although it might be objected that zero-point energy corrections and thermal corrections to the free energy for the two NHase active-site models were calculated in the gas phase using truncated models (Figure S1, Supporting Infor-

(65) For calculations examining substrate selectivity, assuming that nitriles do bind directly to the metal during catalytic turnover, see: Desai, L. V.; Zimmer, M. *Dalton Trans.* **2004**, 872−877.

(66) Rösch, N.; Trickey, S. B. *J. Chem. Phys.* **1997**, *106*, 8940−8941.

mation), this approximation merely assumes that major differences between the vibrational frequencies of **2** and **4** involve the exchangeable ligand and atoms directly bound to the metal center. Such an assumption is supported by the results of NBO analysis (see above), which demonstrate that only the metal−ligand bonds in the truncated active-site structures are substantially affected by variations in the ligand occupying the sixth coordination site.

The next step in this analysis was to evaluate the pK_a of the metal-bound water molecule in active-site model **2** to yield **3** (Scheme 3A). These calculations employed well-established procedures based on a standard thermodynamic cycle (Scheme 3B).[45] Once again, zero-point energy corrections and thermal corrections to the gas-phase energy of NHase model **3** were calculated using a truncated model (Figure S1). Although some error is introduced into the DFT calculations by the difference in the B3LYP self-interaction energy of the charge neutral (**2**) and negative (**3**) NHase active-site models, this is minimized by the size of the structures employed in these calculations.[66] In our calculations on the NHase active-site models, values of −263.9 and −6.28 kcal/mol were chosen for the energy released on transferring a proton from the gas phase to aqueous solution (ΔG_{solv})[46] and the free energy of a proton in the gas phase, respectively.[47] The free energy change for deprotonation of **2** was calculated to be +16 kcal/mol (Table S9), which corresponds to a theoretical pK_a value of 11.7 for the metal-bound water molecule. Although we recognize that such pK_a calculations may have significant error,[45,67] because the Tissandier value for the proton solvation free energy (used herein) is generally accepted as reasonable, the majority of any error likely stems from calculating differences in the continuum solvation energies of the charge neutral (**2** and **4**) and anionic (**3**) NHase models.

Given the free energy differences between **2** and **4** (ΔG = +7.2 kcal/mol) and the pK_a of **2** (ΔG = +16.0 kcal/mol), replacing hydroxide in **3** by acetonitrile to give **4** is calculated to be a thermodynamically favorable reaction for which ΔG = −8.8 kcal/mol (Scheme 1). This reflects, at least in part, the fact that hydroxide is better solvated than acetonitrile in aqueous solution.

Mechanistic Implications of These Theoretical Studies. Systematic, well-defined biochemical studies on the mechanism employed by NHase to catalyze the hydration of nitriles to primary amides have not yet been reported. Efforts to address the role of the metal in catalysis have, therefore, primarily involved the preparation and characterization of inorganic Fe- and Co-containing model complexes. In one plausible mechanism, the nitrile displaces either metal-bound water (model **2**) or hydroxide (model **3**) to yield a new complex in which the substrate is activated toward nucleophilic attack by water (Scheme 1). The observation of spectroscopic shifts when nitriles are added to solutions of the resting enzyme provides support for this proposal.[4a] Unfortunately, such spectral changes might merely reflect a perturbation of the local protein environment caused by substrate and/or inhibitor binding to sites located close to the Fe(III) center. In this regard, we note that INDO/S calculations on active-site model **4** do reproduce these effects when acetonitrile occupies the sixth coordination site about the metal, and although exchange of acetonitrile for water is computed to be thermodynamically unfavorable, this is consistent with a model in which enzymes lower activation-energy barriers by destabilizing the substrate as well as by stabilizing the transition state.[68] The calculated increase in the energy of **4** relative to that of **2** is, however, less than the energy barrier of +13.8 kcal/mol determined in experimental studies of NHase-catalyzed propionitrile hydration,[69] and ligand exchange might be expected to be more energetically favorable for lipophilic nitriles that are less well solvated in water than acetonitrile. Our estimates of ligand-exchange energies also suggest that it is thermodynamically favorable for nitriles to displace hydroxide from the NHase Fe(III) center.

This mechanistic proposal (Scheme 1) suffers, however, from a number of problems, which have been extensively discussed in the literature.[5,6a] First, only one five-coordinate Fe(III) complex that is a model of the NHase metal center has been shown to bind nitriles reversibly, giving a six-coordinate species in which the nitrile is coordinated trans to a thiolate ligand,[19] although this complex does not convert nitriles to primary amides under any conditions yet investigated. On the other hand, these experiments did show the importance of the trans thiolate in increasing the slow ligand-exchange rates that are often observed for low-spin Fe(III) complexes.[19,70] Second, the extent to which the Fe(III) center in NHase can function as a Lewis acid has also been questioned, given the electron-donating character of the deprotonated amide and thiolate ligands,[5] although this might be offset by sulfur oxidation and hydrogen-bonding interactions with the active-site arginine residues.[12b,52] On this point, we note that even given the relatively low value of the NPA-based partial charge computed for the metal in all three active-site models **2**−**4** (Table 4), binding acetonitrile to the Fe(III) center causes the NPA-derived partial charge on the central carbon of the substrate to change from +0.28 to +0.47 $|e^-|$.

Given these issues, a number of alternate mechanisms have been proposed that depend on the coordination of the Fe(III) center by hydroxide in the resting form of active NHase.[5,6a,10a] For example, the metal-bound hydroxide might function as a general base catalyst to activate water for nucleophilic addition to the nitrile moiety, thereby avoiding the direct binding of substrate, reaction intermediates, or amide product with the Fe(III) center. Alternatively, the metal-bound hydroxide might attack the nitrile to form an Fe-bound imidate intermediate that dissociates to give a five-coordinate intermediate that can bind water prior to the loss

(67) Jang, Y. H.; Sowers, L. C.; Cagin, T.; Goddard, W. A., III. *J. Phys. Chem. A* **2001**, *105*, 274−280.
(68) Schramm, V. E. *Annu. Rev. Biochem.* **1998**, *67*, 693−720.
(69) Alfani, F.; Cantarella, M.; Spera, A.; Viparelli, P. *J. Mol. Catal.* **2001**, *11*, 687−697.
(70) Shearer, J.; Kung, I. Y.; Lovell, S.; Kaminsky, W.; Kovacs, J. A. *J. Am. Chem. Soc.* **2001**, *123*, 463−468.

of a proton and formation of the resting form of the enzyme. These mechanistic possibilities, however, require the presence of hydroxide in the sixth coordination site, in contradiction to our finding that active-site model **2** possesses calculated structural, electronic, and spectroscopic properties that are more consistent with experimental observations of active NHase than those computed for **3**. In addition, the pK_a of water in active-site model **2** is predicted to be 12.9 in these theoretical studies, ruling out substantial amounts of the hydroxide-bound form of NHase at, or just below, neutral pH. Even given the considerable difficulties inherent in computing absolute pK_a values,[71] the computed value is consistent with the reduced Lewis acidity that has been postulated for the electron-rich NHase Fe(III) center.[5]

In light of these computational results and their implications for our mechanistic understanding of NHase, we reexamined the experimental studies supporting the presence of Fe-bound hydroxide in the active site of the enzyme. The most convincing evidence for this hypothesis has been provided by determining the signs of hyperfine couplings in Mims electron spin−echo (ESE) ENDOR measurements on resting, uniformly labeled ^{15}N−NHase.[72] Thus, ENDOR experiments on the enzyme in the presence of ^{17}O-labeled water lead to the detection of two exchangeable protons (X1 and X2) that were assigned as being on the Fe-bound water molecule.[73] Subsequent analysis of the ESE ENDOR spectra, however, showed that this could not be the case because the hyperfine couplings of X1 and X2 were of opposite sign, leading to the conclusion that one of the protons was on metal-bound hydroxide and the other was associated with an ionizable group in the protein active site. Unfortunately, these conclusions were made prior to the determination of high-resolution NHase crystal structures and employed an incorrect model for the ligands coordinating Fe(III). Thus, it is quite possible that hydrogen-bonding interactions between the Ser-113 side chain and the metal-bound water might slow the exchange of one of the solvent protons under the conditions of the experiment. In addition, the samples of the enzyme that were used to obtain the EPR spectra contained butyric acid,[16,73] complicating data interpretation, given that the carboxylate moiety can likely bind to the Fe(III) center of the enzyme, as observed for the Co-containing NHase from *Pseudonocardia thermophila* JCM 1095.[2f] A second piece of evidence supporting an Fe-bound hydroxide in resting NHase has been provided by spectroscopic studies of an Fe(III) complex in which the metal is coordinated by deprotonated amide and thiolate ligands. These experiments showed that the pK_a of metal-bound water in this compound was 6.3 ± 0.4,[20a] consistent with the proposal that hydroxide occupies the sixth coordination site in resting NHase at physiological pH. On the other hand, the effects of a protein environment are not adequately modeled in such studies, andFe-dependent NHase activity is abolished as the solution pH is increased from 7 to 9.[17] If metal-bound hydroxide were a catalytically important species, then increasing the solution pH might be expected to give more of this enzyme form. Such an interpretation is complicated, however, by possible deprotonation of a protein side chain that functions in general acid catalysis or nitrile binding. Given these problems in interpreting the implications of these experimental observations for the mechanism of NHase, our pK_a calculation cannot be regarded merely as an artifact arising from limitations of our active-site models.

Resonance Raman (RR) spectroscopy has also been used to investigate the nature of the sixth ligand in the active enzyme, at excitation wavelengths of 413,[7b] 640,[2d] and 714 nm.[17] On the basis of our DFT calculations, electronic excitations involving either the Fe d_{yz} and d_{z^2} orbitals might be expected to show resonance-enhanced vibrations for the Fe−OH stretching mode if hydroxide were the sixth ligand, because excitations in both the low-energy region (∼600−675 nm) and 400-nm region involve molecular orbitals having significant Fe−OH character. In this regard, no RR study has shown an absorption corresponding to an Fe−OH stretching mode, and no ^{18}O isotopic shifts consistent with bound hydroxide were observed in experiments employing excitation at 714 nm.[17] The interpretation of these studies is further complicated by the fact that the NHase used in these experiments was purified in the presence of butyric acid at concentrations of either 20[7b] or 40 mM.[2d,17] This additive is a competitive inhibitor of the Fe-dependent NHase, rendering it inactive at concentrations of 40 mM or higher,[2e] and butyrate binds directly to the metal center of Co-dependent NHase.[2f] Therefore, experimental RR spectra either represent the butyrate-inhibited form of NHase or a mixture of solvent- and butyrate-bound forms of the Fe(III) center, resulting in the resonance-enhanced vibrations of an Fe−OH stretch becoming unresolvable.

In summary, although we recognize that our computational strategy has limitations, these DFT calculations of Fe(III) spin-state energetics and water pK_a in active-site model **2**, together with the INDO/S spectra calculated for the three models, re-open the possibility that water is the sixth metal ligand in the resting form of active NHase. In addition, whether water or hydroxide coordinates Fe(III) in the active site, they do not rule out direct coordination of the nitrile to the metal during catalytic turnover. Perhaps more importantly, our studies indicate that experimental investigations remain to be performed on NHase under strictly controlled conditions. For example, although there may be an impact on enzyme stability, detailed spectroscopic characterization of the NHase Fe(III) center in the absence of butyrate, using both optical and EPR methods, will be essential to calibrate the structural and mechanistic implications of our computational findings.

(71) (a) Simonson, T.; Carlsson, J.; Case, D. A. *J. Am. Chem. Soc.* **2004**, *126*, 4167−4180. (b) Kuhn, B.; Kollman, P. A.; Stahl, M. *J. Comput. Chem.* **2004**, *25*, 1865−1872. (c) Mehler, E. L.; Fuxreiter, M.; Simon, I.; Garcia-Moreno, B. *Proteins: Struct., Funct., Genet.* **2002**, *48*, 283−292. (d) Bashford, D.; Karplus, M. *Biochemistry* **1990**, *29*, 10219−10225. (e) Bashford, D. *Front. Biosci.* **2004**, *9*, 1082−1099.

(72) Doan, P. E.; Nelson, M. J.; Jin, H.; Hoffmann, B. M. *J. Am. Chem. Soc.* **1996**, *118*, 7014−7015.

(73) Jin, H.; Turner, I. M., Jr.; Nelson, M. J.; Gurbiel, R. J.; Doan, P. E.; Hoffmann, B. M. *J. Am. Chem. Soc.* **1993**, *115*, 5290−5291.

(74) Purvis, G. D.; Sekino, H.; Bartlett, R. J. *Collect. Czech. Chem. Commun.* **1988**, *53*, 2203−2213.

(75) Wendt, M.; Weinhold, F. *NBOView 1.0*; Theoretical Chemistry Institute, University of Wisconsin: Madison, WI, 2001.

Acknowledgment. We thank the National Science Foundation (CHE-0079008) for their support of this work and the National Partnership for Advanced Computational Infrastructure (NPACI) for the provision of supercomputing facilities. We also acknowledge Dr. Marshall Cory, Jr., for developing the software package used to perform Gaussian broadening of the calculated INDO/S electronic transitions.

Supporting Information Available: Complete citation for ref 30, Tables S1−S9, Figures S1−S4 showing the truncated models employed in zero-point energy evaluations, and graphical representations of the MOs involved in the electronic transitions listed in Tables S6−S8. This material is available free of charge via the Internet at http://pubs.acs.org.

IC050965P